Chromium Isotope Constraints on the Mid-Proterozoic Redox: Evidence from $\delta^{53}Cr$ of Carbonates from the greater McArthur Basin, Northern Australia

Thesis Submitted in Accordance with the requirements of the University of Adelaide for an Honours Degree in Geology

2018 Geoscience Honours Thesis

Geremiah Emmanuel Toledo

Word Count: 6461

2 Equations, 3 Tables and 23 Figures

THE UNIVERSITY of ADELAIDE

CHROMIUM ISOTOPE CONSTRAINTS ON THE MID-PROTEROZOIC REDOX: EVIDENCE FROM δ^{53}CR OF CARBONATES FROM THE GREATER MCARTHUR BASIN, NORTHERN AUSTRALIA

RUNNING TITLE

Cr Isotope Constraints on Mid-Proterozoic Redox Conditions

ABSTRACT

The Great Oxygenation Event (GOE) and the Neoproterozoic Oxygenation Event (NOE) are interpreted to have made the most profound and permanent surface redox changes in Earth's history. Changes in redox conditions between these two oxygenation events (i.e. mid-Proterozoic; 1.8-0.8 Ga), are poorly understood, where environmental stability with persistently low atmospheric oxygen is assumed (<0.1% PAL; Present Atmospheric Levels). This period also witnessed the first appearance of primitive eukaryotes, however *Eukarya* diversification was determined to be effectively stagnant presumably due to sustained low atmospheric oxygen levels (pO_2). More recent studies found evidence of relatively high mid-Proterozoic pO_2, well in excess of 1% PAL, sufficient to promote diversification. The importance of better understanding the past redox conditions heightens, due to the contrasting pO_2 estimates that plausibly swayed the *Eukarya* diversification.

This study presents stable Cr isotope (δ^{53}Cr) values, in mid-Proterozoic organic-rich carbonates of the Limbunya and McArthur Groups from the greater McArthur Basin. Analysed values from -0.293‰ to +1.389‰, present the oldest documented positively fractionated mid-Proterozoic δ^{53}Cr values in marine carbonate units *ca.* 1.64 Gyrs ago, suggestive of a fluctuating, but increasing pO_2 at the time of a generally reducing environment; supporting a permissive environment for *Eukarya* diversification. However, it is likely that its unstable nature probably inhibited wider and earlier *Eukarya* diversification, should pO_2 levels truly be a barrier for evolution.

KEYWORDS

Chromium Isotopes, Paleo-Redox, mid-Proterozoic, Carbonates, Shales, McArthur Basin

TABLE OF CONTENTS

LIST OF FIGURES AND TABLES

INTRODUCTION

Cumulating evidence over the past decade have effectively established that the Great Oxygenation Event (GOE, *ca.* 2.40 Ga), and the Neoproterozoic Oxygenation Event (NOE, *ca.* 0.64 Ga) resulted in permanent redox changes and oxygenation of the Earth's surface environments (Bekker *et al.*, 2004; Frei et al., 2009). Oxygen levels (pO_2) during the GOE are believed to increase by approximately two orders of magnitude from Archean levels of <0.001% PAL (Present Atmospheric Levels) to >0.1% PAL (Holland, 2006; Lyons, Reinhard, & Planavsky, 2014), and the subsequent NOE increased atmospheric pO_2 to levels approaching modern conditions (Tang *et al.*, 2016). However, the redox conditions of the ocean-atmosphere system during the time interval between the GOE and NOE (i.e. mid-Proterozoic; *ca.* 1.8-0.8 Ga) remains poorly understood, but it is assumed that atmospheric pO_2 remained stable and relatively low throughout (≤0.1% PAL; (Lyons et al., 2014; Planavsky et al., 2014; Tang et al., 2016). This period also witnessed the first appearance of structurally-complex primitive eukaryotes, although, *Eukarya* diversification was limited during this period (Lamb *et al.*, 2009; Zhu *et al.*, 2016), presumably inhibited by low pO_2 levels (Planavsky et al., 2014; Tang et al., 2016). Conversely, more recent paleo-redox studies insinuate relatively high mid-Proterozoic pO_2, well in excess of 1% PAL, which would be sufficient to promote *Eukarya* diversification (Canfield et al., 2018; Cox *et al.*, 2016; Zhang *et al.*, 2016).

These divergent views and reconstructions of atmospheric oxygen levels during the mid-Proterozoic need to be addressed by new and detailed paleo-redox studies, due to their significant implications not only for the timing of *Eukarya* diversification but also

to better understand Earth's surface oxygenation (Cole et al., 2016; Gilleaudeau et al., 2016; Lyons et al., 2014). Therefore, investigating the redox conditions during the mid-Proterozoic via stable Cr isotopes can provide key evidence to further resolve the physical and temporal conditions of complex *Eukarya* development.

To help address these uncertainties, this study analysed stable Cr isotopes ($\delta^{53}Cr$) to mid-Proterozoic sedimentary units from the greater McArthur Basin, as a paleo-redox proxy for the ancient ocean-atmosphere system. Specifically, the $\delta^{53}Cr$ isotopic values were measured in carbonate and shale samples taken from the Paleoproterozoic Limbunya and McArthur Groups in two distal correlative drill cores (i.e. Manbulloo S1 and LV09001 drill cores) to determine whether fractionated $\delta^{53}Cr$ values are preserved in *ca*. 1.64 Ga rocks.

Chromium Isotopic System as a Redox-Sensitive Proxy

The ratio of $^{53}Cr/^{52}Cr$ in authigenic sedimentary rocks and minerals, expressed as $\delta^{53}Cr$, is a novel and sensitive tracer for past pO_2 levels in the ocean-atmosphere system as the fractionation of Cr isotopes at surface conditions is redox-dependent (Ellis, Johnson, & Bullen, 2002; Saad *et al.*, 2017). Cr occurs in its trivalent oxidation state in igneous minerals where it is insoluble under most conditions, found to have a limited $\delta^{53}Cr$ signature of $-0.124 \pm 0.101‰$ (i.e. reflecting crustal/silicate Cr reservoirs; (Schoenberg *et al.*, 2008). During oxidative terrestrial weathering, stable Manganese-oxyhydroxides (MnO_2) catalytically oxidise insoluble Cr(III) to its relatively soluble hexavalent state, Cr(VI); enriched in heavy ^{53}Cr after partial reduction of the latter chromate anions (Frei et al., 2009; Gilleaudeau et al., 2016), providing a unique Cr isotope signature to trace oxidative weathering in modern settings and past geological

records. These positively fractionated Cr isotope values generated via oxidative terrestrial weathering are subsequently transported by rivers and streams (as dissolved chromate anions) into the oceans, eventually becoming incorporated in marine sediments with positive δ^{53}Cr values (Figure 1; (Cole et al., 2016; Holmden et al., 2016).

The residence time of Cr in modern oceans, is estimated at *ca.* 9 – 40 kyrs, representing the average time Cr spends in seawater as dissolved Cr(VI) species before being reduced to Cr(III) by anoxic bottom waters, microbes, Fe(II), or incorporated directly as Cr(VI) species into marine sediments (Holmden et al., 2016). Fractionated Cr is then deposited in marine sediments with isotope values that are positively fractionated compared to igneous crustal values. Therefore, high-temperature conditions or crustal sources should reflect limited chromium isotope fractionation, while low-temperature redox processes, associated with oxidising conditions, should produce isotopically heavier values in dissolved seawater Cr reservoir and associated marine sediments.

In addition, Frei et al. (2016) proposed oxygen threshold values required to stabilise MnO_2 and oxidise Cr could be as low as 0.001% PAL. Kinetic considerations, however, state that 0.1 – 1% PAL is sufficient to oxidise Cr, considering usual soil-residence time; and levels between 0.03 – 0.3% PAL are adequate to prevent reduction of Cr(VI) by Fe(II) during riverine transport (Frei et al., 2016). These pO_2 threshold values make Cr isotopes a highly-sensitive paleo-redox tracer.

Recent studies found that δ^{53}Cr fractionations in marine settings can also occur from processes such as: a) microbial reduction; b) Fe(II) reduction; c) ligand-complexation fractionation; d) sediment exchange; e) carbonate uptake; f) influences of igneous provinces (Figure 1); and g) detrital phases on marine Cr isotope budget. These specific

processes and their effects on Cr isotope fractionation are described in more detail below.

a) Microbial reduction is a process independent of oxidative terrestrial weathering, found to occur in both fluvial and marine environments, where microbes can partially fractionate $\delta^{53}Cr$ by as much as $-4.1‰$; further enriching the chromium delivered into the oceans with heavier isotopes (Frei et al., 2009; Moos, 2018). Sedimentary denitrification associated with microbial reduction was found to strongly correlate with $\delta^{15}N$ where both Cr and N elements are simultaneously found to be isotopically lighter (Gueguen et al., 2016; Moos, 2018).
b) Similarly, Fe(II)-rich sediments in fluvial and marine systems are potent reductants for chromium, preferentially adsorbing lighter chromium isotopes onto particles, and thus enriching the water column with heavier Cr isotopes, should partial reduction occur (Cole et al., 2016; Ellis et al., 2002; Gilleaudeau et al., 2016).
c) Saad et al. (2017) reported isotopic fractionation through ligand-complexation can occur in the marine environment, independent of redox processes. Although prematurely understood, fractionations observed from organic acids and siderophores ranged from -0.27 to $+1.23‰$ (Saad et al., 2017). However, Canfield et al. (2018) stated that such effect was unlikely to influence the current view of the association of pO_2 levels with $\delta^{53}Cr$ values in Proterozoic sediments.
d) Sediment exchange was found to positively fractionate chromium, where the Cr in the upper pore waters and top sediment layer is exchanged with the Cr in the water column. This preferentially removes lighter isotopes resulting in heavier isotopes residing in the water column. Such a process was found to increase the Cr concentration in bottom waters while Cr concentrations in the pore waters

simultaneously decrease (Moos, 2018). Holmden et al. (2016) summarised such a process can fractionate δ^{53}Cr by as much as $+0.5$ to $+1.5$‰. These upper sediment pore waters can be anoxic and contain acid volatile sulphides that can potentially reduce Cr (Graham & Bouwer, 2010).

e) Carbonate uptake and biomineralisation processes can preferentially remove either lighter or heavier Cr isotopes from the seawater, rendering such process to be largely unconstrained. Carbonates can directly incorporate Cr as CrO_4^{2-} and/or $Cr(H_2O)_6^{3+}$ in its crystal lattice during precipitation (Holmden et al., 2016; Rodler et al., 2015).

f) Weathering of large igneous provinces (LIPs) by riverine systems were found to influence δ^{53}Cr fractionations and Cr isotope budget in the oceans, where rivers underlain by ultramafic rocks produce the highest δ^{53}Cr values as well as highest Cr concentrations (Frei, Poiré, & Frei, 2014). Whereas, rivers underlain by more felsic rocks produce smaller fractionations (Frei et al., 2014).

g) Gilleaudeau et al. (2016) and Farkaš *et al.* (2018) reported that detrital Cr can produce values in carbonates that are similar to the crustal values, where more detrital components in sediments result to δ^{53}Cr values approaching -0.124‰. This fractionation is not caused by a process, *per se*, rather as an effect of sample impurities.

Although plentiful variables controlling Cr isotope fractionation in modern and past Earth surface environments remain uncertain, the net result of Cr redox cycling in oxidative terrestrial weathering environments should still produce positive δ^{53}Cr values heavier than those observed in igneous crustal Cr reservoirs or Bulk Silicate Earth (Holmden et al., 2016).

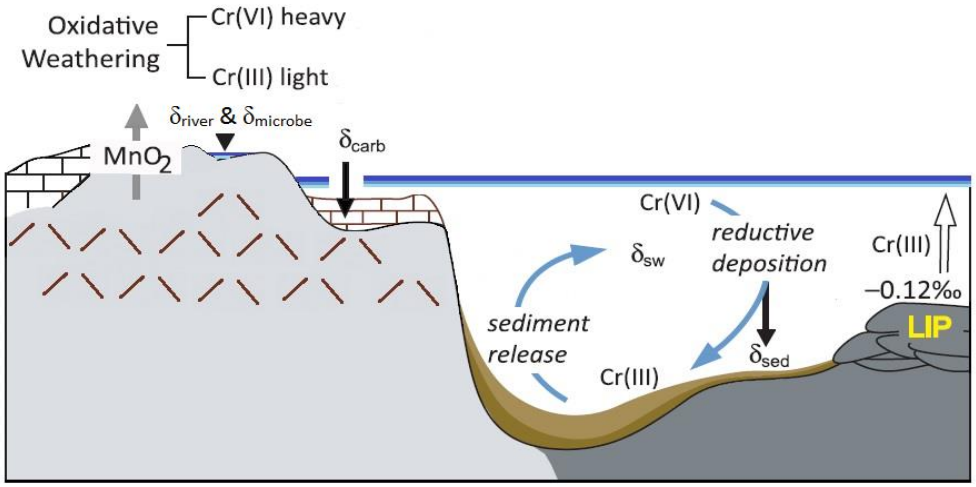

Figure 1. Cr redox cycle including some redox processes, adapted from Holmden et al. (2016) where 'SW' means seawater; 'carb' means carbonates; 'sed' means sediments; and 'LIP' means Large Igneous Province.

The greater McArthur Basin contains a variety of shallow to deeper marine sedimentary units with mid-Proterozoic ages (B. Yang *et al.*, 2018). Therefore, Cr isotope analysis on suitable and well-preserved units (e.g. carbonates and shales) from this unique basin can help estimate the redox conditions of the ocean-atmosphere system during the mid-Proterozoic. This study presents a world first evidence of positively fractionated $\delta^{53}Cr$ values in *ca.* 1.64 billion year old carbonates from the greater McArthur Basin, exceedingly higher and stratigraphically older compared to any previously published Cr isotope data from this time interval. These $\delta^{53}Cr$ data provide evidence for enhanced pO_2 levels and less reducing conditions in the greater McArthur Basin, which in turn provide new constraints on the paleo-redox conditions leading to *Eukarya* diversification. The *biota* likely thrived and produced sufficient amounts of oxygen, possibly slightly more than previously modelled, in otherwise predominantly reducing and oxygen-depleted conditions of mid-Proterozoic oceans.

GEOLOGICAL SETTING

Greater McArthur Basin

The greater McArthur Basin is an informally termed Proterozoic basin system located in northern Australia, containing Paleoproterozoic to Neoproterozoic sedimentary cover (B. Yang et al., 2018). The Birrindudu and McArthur Basins are only two of the multiple basins and sub-basins identified, collectively making up the 'greater McArthur Basin' (Figure 2). All rock samples analysed in this project originated from the McArthur (McArthur Basin), and the Limbunya Groups (Birrindudu Basin).

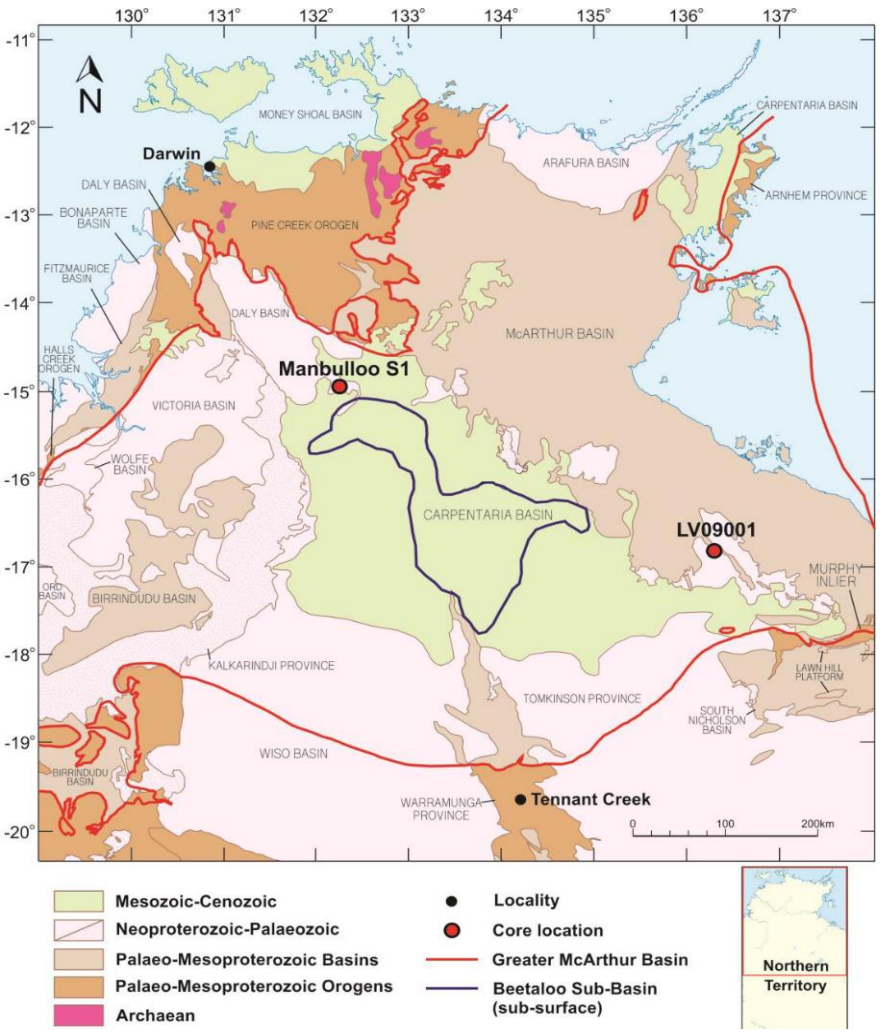

Figure 2. Geological map of Northern Australia with locations of studied cores (Manbulloo S1 and LV09001), adapted from Bullen (2017).

LIMBUNYA GROUP – SEDIMENTARY RECORD FROM MANBULLOO S1 DRILL CORE

The Statherian-aged Paleoproterozoic Limbunya Group (Figures 3 and 4) in the Birrindudu Basin (Figure 2) is part of an organic-rich carbonate-dominated package. The presence of stromatolitic carbonates and black shales signify shallow-to-moderately deep marine depositional settings (Bullen, 2017). The formations analysed ranged from the Blue Hole Formation (oldest) to the Undifferentiated Upper McArthur (youngest). The sedimentology of the formations as well as C and Sr isotope constraints from carbonates in this core suggest possible 'basinal restriction events' around 1.64 Ga, associated with the deposition of organic-rich facies (Bullen, 2017).

BLUE HOLE FORMATION, LIMBUNYA GROUP

The oldest Limbunya unit analysed, the ***Blue Hole Formation***, is a dolomitic mud-rich siltstone with minor tuffite, representing a shallow-to-moderately deep marine depositional environment, proximal to a volcanic zone.

CAMPBELL SPRINGS DOLOMITE, LIMBUNYA GROUP

The conformably overlying ***Campbell Springs Dolomite*** (CSD) is a stromatolitic carbonate unit with rare sandstones, signifying a shallow marine environment (Bullen, 2017).

FRAYNES FORMATION, LIMBUNYA GROUP

Conformably overlying the CSD, the 1638 ± 9 Myr ***Fraynes Formation*** (Bullen, 2017), consists of laminated organic-rich shales and dolomitic siltstones, with an increasing

carbonate proportion upwards, denoting a low-energy anoxic/euxinic shallow-to-moderately deep marine setting.

REWARD DOLOMITE, LIMBUNYA GROUP

Conformably overlying the Fraynes Formation, the younger ***Reward Dolomite*** consists of predominantly dolomitic sandstone and dolostone with evaporite pseudomorphs, indicating an evaporative shallow lagoon/marine environment (Bullen, 2017).

UNDIFFERENTIATED UPPER MCARTHUR, LIMBUNYA GROUP

Conformably overlying the Reward Dolomite, the ***Undifferentiated Upper McArthur*** is a dolomite-rich unit of interbedded sand and silt (Bullen, 2017), implying a depositional environment proximal to the shoreline.

Collectively, the depositional settings throughout the Limbunya Group and its facies reflect shallow-to-moderately deep marine settings controlled by a combination of relative sea-level changes, local redox conditions, and basinal subsidence caused by tectonic processes in central Australia at the time (Bullen, 2017).

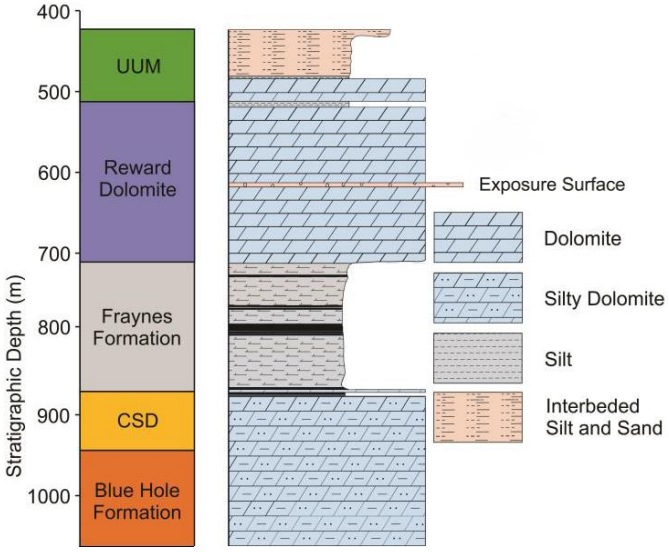

Figure 3. Stratigraphic log of the Manbulloo S1 drill core, classified by Bullen (2017) where 'CSD' means Campbell Springs Dolomite and 'UUM' means Undifferentiated Upper McArthur.

McArthur Group – Sedimentary record from LV09001 Drill Core

The Statherian-aged Paleoproterozoic McArthur Group is one of the four main groups in the McArthur Basin containing formations from the Emmerugga Dolomite (oldest) to the Donnegan Member (youngest; Figures 4 and 5). Informally, it is the geological equivalent of the Limbunya Group from the eastern parts of the greater McArthur Basin.

EMMERUGGA DOLOMITE, MCARTHUR GROUP

The oldest McArthur unit analysed, the ***Emmerugga Dolomite***, is a karstic carbonaceous unit, demonstrating a shallow marine/lagoonal environment (Guiliano, 2016). Informally, it is the eastern geological equivalence of the Blue Hole Formation (Limbunya Group) due to its similarity in ages, sedimentology and geochemical properties (Bullen, 2017).

TEENA DOLOMITE MEMBER, MCARTHUR GROUP

Conformably overlying the Emmerugga Dolomite, the ***Teena Dolomite Member*** contains evaporite pseudomorphs and stromatolites in the upper interval as well as karst features. Jointly with the Emmerugga Dolomite, they were interpreted to record a basinal regression event (Guiliano, 2016). Its silica-rich matrix is a possible post-diagenetic event of Si-rich fluid infill. It is the informal eastern equivalence of the CSD (Bullen, 2017).

COOLEY BRECCIA MEMBER, MCARTHUR GROUP

The younger overlying ***Cooley Member*** contains brecciated debris flows of the older Teena Member and Emmerugga Dolomite (Guiliano, 2016), connoting a steeply sloping marine depositional environment.

BARNEY CREEK FORMATION, MCARTHUR GROUP

The 1638 ± 3 Myr ***Barney Creek Formation*** (BCF) in the McArthur Group conformably overlies the Cooley Member, predominantly comprising thinly organic-rich mudstone with minor pyrite present throughout the lithology (Baruch *et al.*, 2015), confined in rare massively jigsaw-brecciated sections. Presumably, an uplift and minor rifting caused basinal subsidence which resulted in accommodation space essential for a low-energy anoxic depositional environment in a redox-stratified marine/lagoonal setting (Guiliano, 2016); exceptionally preserving the organic-rich sediments (Baruch et al., 2015). Its similar ages, geochemical properties and sedimentology corresponds to the Fraynes Formation from the western parts of the greater McArthur Basin (Bullen, 2017).

REWARD DOLOMITE, MCARTHUR GROUP

The BCF is transitionally and conformably overlain by the ***Reward Dolomite*** (e.g. karst features and rare breccia; (Baruch et al., 2015; Guiliano, 2016), denoting a shallow marine depositional setting close to a terrestrial environment. Some sections are dominated by large silicified grains supported by carbonate-rich matrix while others are dominated by spheroidal microfossils supported by an organic-rich matrix (Guiliano, 2016).

HOT SPRINGS MEMBER, MCARTHUR GROUP

The younger ***Hot Springs Member*** is a stromatolitic and highly-silicified dolostone interbedded with silicified evaporites (Guiliano, 2016), implying an evaporative depositional setting and later alteration of carbonates and evaporites by Si-rich fluids.

DONNEGAN MEMBER, MCARTHUR GROUP

The youngest McArthur unit analysed, the ***Donnegan Member***, overlies the Hot Springs Member and is mainly a greyish green dolomitic-siltstone with sandy layers confined in the upper section, signifying a depositional environment proximal to the shoreline (Guiliano, 2016).

In summary, available $\delta^{13}C$ and $^{87}Sr/^{86}Sr$ data from Bullen (2017) and Guiliano (2016) suggest that the depositional settings of these sedimentary records from the McArthur Group reflect synchronous 'basinal restriction events' from a relatively open marine setting (Figure 4; Teena and Reward Dolomites), where the proposed basinal restrictions were most pronounced during deposition of organic-rich shale facies (BCF and Fraynes Formation; Figure 5). Such a restriction event was also thought to cause water and redox stratifications in the basin (Bullen, 2017; Guiliano, 2016), which in turn might have controlled the preservation and abundance of organic matter. In addition, the geological similarities of the Limbunya and the McArthur Groups support the model of connected different sub-basins within the greater McArthur Basin, and their respective $\delta^{13}C$ and $^{87}Sr/^{86}Sr$ trends, as supported by data from Manbulloo S1 and LV09001 drill cores and their correlated isotope trends across the basin.

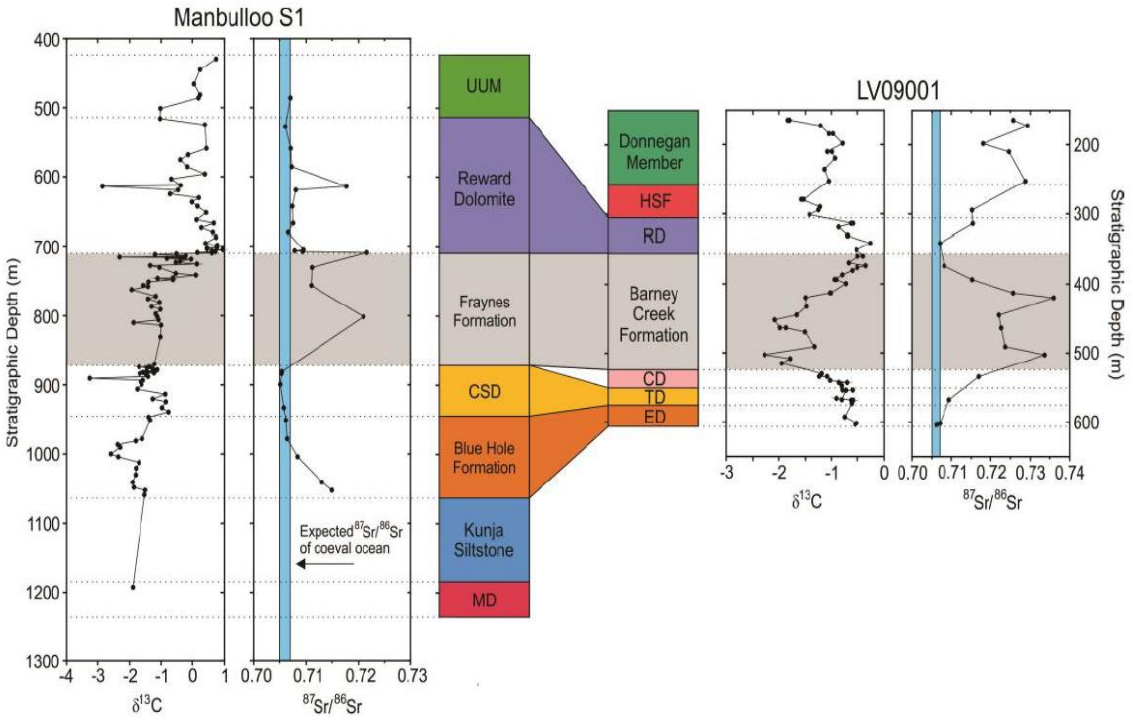

Figure 4. Comparison of key geochemical features from Manbulloo S1 and LV09001 drill cores. Both cores contain more radiogenic $^{87}Sr/^{86}Sr$ and negative $\delta^{13}C$ ratios during Fraynes and Barney Creek Formation depositions. The data from LV09001 were taken from Guiliano (2016), with the whole image taken from Bullen (2017). 'CSD' means Campbell Springs Dolomite, 'UUM' means Undifferentiated Upper McArthur, MD means Mallahbah Dolostone, CD means Cooley Dolostone, TD means Teena Dolostone and ED means Emmerugga Dolostone.

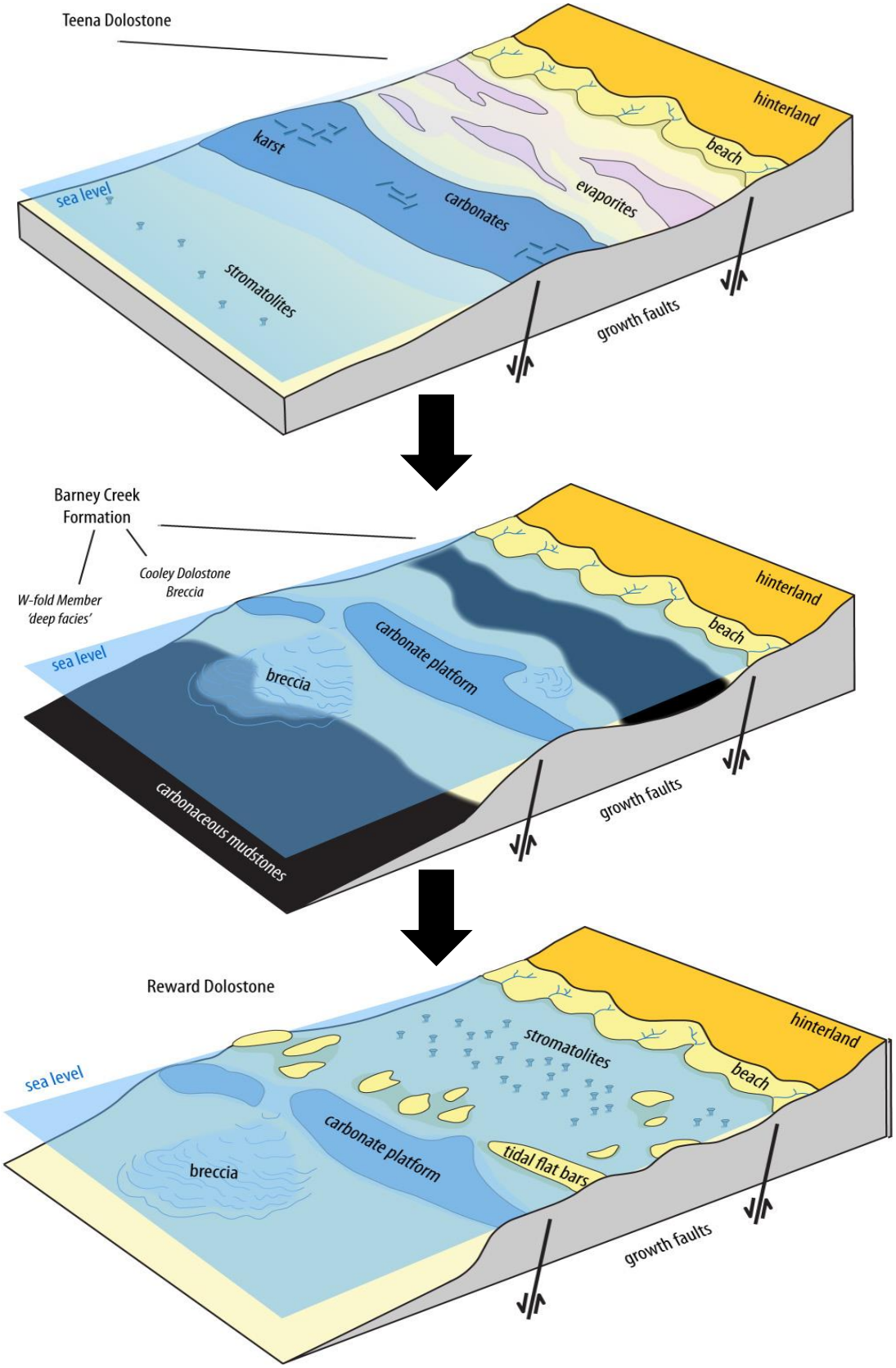

Figure 5. ***ca.*** **1.64 Ga 'Basin Regression' progression model based on the depositional settings of the McArthur Group formations, adapted from Schmid (2015).**

METHODOLOGY

Drill Core Sampling and Selection

Samples from the McArthur and Limbunya Groups were obtained from the LV09001 and Manbulloo S1 drill cores, respectively (Figure 2). Access and permission to samples were provided by the Northern Territory Geological Survey. In general, these drill cores indicate very little to no post-depositional alteration of carbonates and shales, excluding the brecciated and silicified units in LV09001 core, containing complete and undisturbed record of mid-Proterozoic environmental changes in the greater McArthur Basin, making these sedimentary units ideal targets for geochemical and isotope analyses. All rock samples (quarter core sections and/or rock chips) were powdered by a Rocklabs Tungsten Carbide Ring Mill, avoiding contact of the samples with stainless steel materials, potentially contaminating the samples with Cr and other interfering elements (e.g. Fe, Ti, Mn and V).

Sample Preparation: Chromatography, Double Spiking, and TIMS

Cr was isolated from rock matrices using a ^{50}Cr-^{54}Cr double spiked Cr-purification chromatography method heavily adapted from Paulukat (2016). The procedure sequentially involved; (i) sample leaching, (ii) ^{50}Cr-^{54}Cr double spiking, (iii) chromatographic purification of Cr from sample matrix (i.e. anion and cation columns, Figure 7) and, (iv) subsequent analysis of Cr isotope abundances by Thermal Ionisation Mass Spectrometry (TIMS). For more details on individual methods, see information and data provided in Supplementary Information.

SAMPLE PREPARATION

Powdered carbonate/shale samples were weighed and initially contain ~0.5µg of Cr. Samples were leached with 20mL of 2N HCl at room temperature for ~24hrs. Approximately 1mL of the leachate was kept for major and trace element analysis using ICP-MS, after being centrifuged. The leachates were subsequently spiked with an appropriate equivalent of ^{50}Cr-^{54}Cr isotope tracer or double spike (DS), prepared at Czech Geological Survey, Prague (see Farkaš *et al.* (2013). These spiked leachates were again centrifuged to filter the carbonates from the silicates as a preparation step (Gilleaudeau et al., 2016; Reinhard *et al.*, 2014). The sample-to-spike ratio was kept closely to unity (1:1 ratio), for every 1000ng of Cr in the sample, an equivalent ~1µL of ^{50}Cr-^{54}Cr DS was added. The leached and spiked samples were then evaporated and re-dissolved with *Aqua Regia* to homogenise the DS. After another evaporation, the samples were re-dissolved in Milli-Q H_2O overnight at room temperature, ready for the first chromatography step, the 'anion column'.

FIRST COLUMN: ANION COLUMN (BIO-RAD AG® 1-X8)

The 'anion column' was pre-cleaned and loaded with anion-exchange resins (Bio-Rad AG® 1-X8; 100-200mesh) calibrated to isolate Cr (as Cr(VI) oxyanion species: CrO_4^{2-}) from other sample matrix elements, particularly interfering metals. The sample solutions were oxidised with ammonium persulfate, $(NH_4)_2S_2O_8$, before being loaded into the anion-exchange resins. The interfering metals such as Fe, Ti, V and Mn were eluted with 0.2N and 2N HCl acid concentrations. This elution step removes interfering elements while Cr remains oxidised and attached onto resin beads as Cr(VI) oxyanion species. After the matrix elution, Cr is collected with 2N HNO_3 and 5% H_2O_2, providing the required acidity and high redox-potential needed to reduce Cr(VI) to

Cr(III), releasing Cr from the resin (Figure 6; (Paulukat, 2016). This step ideally isolates Cr from most matrix elements with some trace quantity remnants.

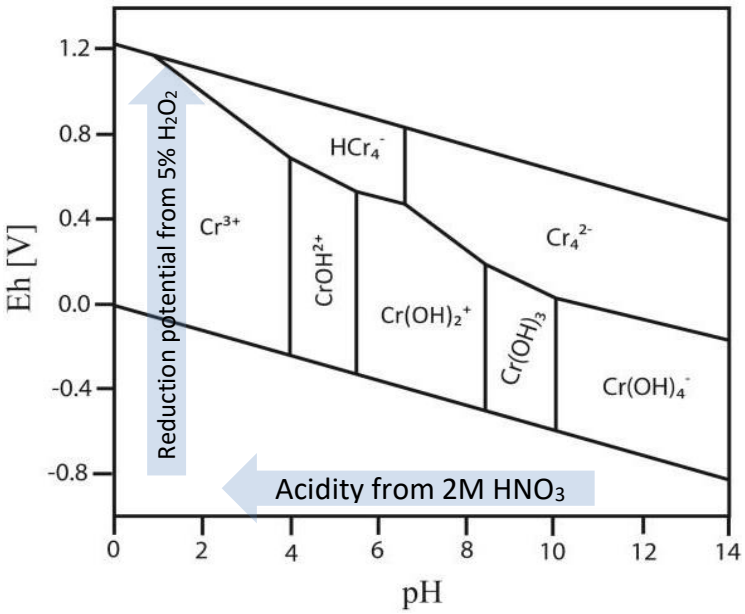

Figure 6. Different Cr oxidation species showing the reduction of Cr(VI) with HNO_3 and H_2O_2 as reductants in the reaction; adapted from Paulukat (2016).

SECOND COLUMN: IRON COLUMN (BIO-RAD AG® 1-X8)

Samples with more than 300ppm of Fe were also passed through a dedicated 'Fe column', having a high affinity for iron but not for other elements (i.e. Fe-specific column). This step uses the same column and resin as the 'anion column' but the rock matrix is eluted with 6N HCl. Samples with lesser Fe-concentrations were not necessarily passed through this second 'Fe column'.

THIRD COLUMN: CATION COLUMN (BIO-RAD AG® 50W-X8)

A third column, the 'cation column', was the *Evergreen Scientific column*, pre-cleaned and loaded with cation-exchange resins (Bio-Rad AG® 50W-X8; 200 − 400mesh) calibrated to separate other remaining elements from chromium (Paulukat, 2016). This

cation-exchange resin adheres the remaining elements, with the final Cr fraction eluted Cr with 0.5N HCl.

A schematic summary of the three-column Cr-Purification procedure, with main steps and acid elution, are illustrated in the flow chart (Figure 7), and a full calibration of both anion and cation columns are also presented in the section below (Figures 8 and 9).

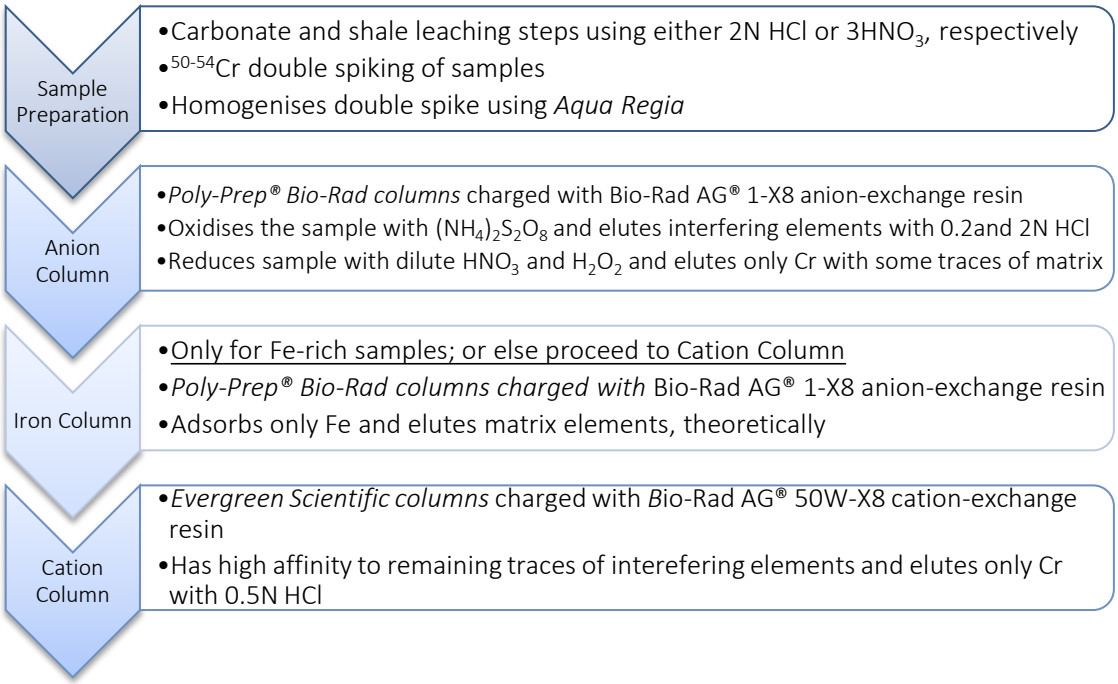

Figure 7. Simplified flow chart of the three-step Cr-Purification Chromatography.

Cr-Purification Chromatography: Full Calibration of Anion and Cation Column

To confirm the robustness and fidelity of the adapted Cr-purification Chromatography, a full calibration test of both anion and cation columns (concentrations of selected elements), were analysed by ICP-MS at the Adelaide Microscopy (see Figures 8 and 9; anion and cation columns, respectively).

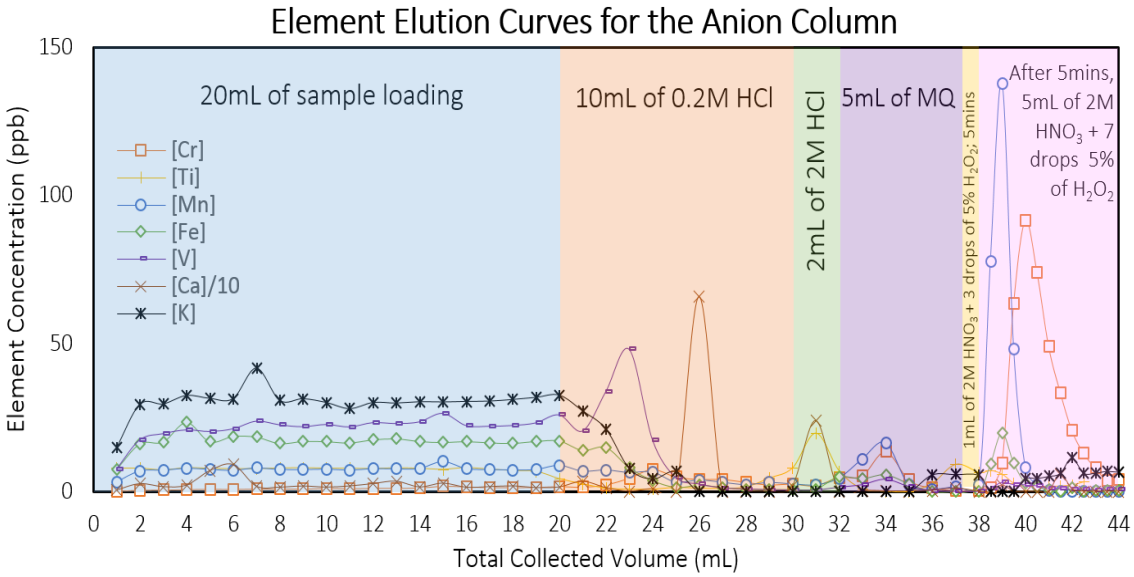

Figure 9. Elemental elution curves of Cr and its interfering elements as well as Ca and K throughout the 'Cation Column' Procedure; where Ca and K represent alkali and alkaline Earth metals.

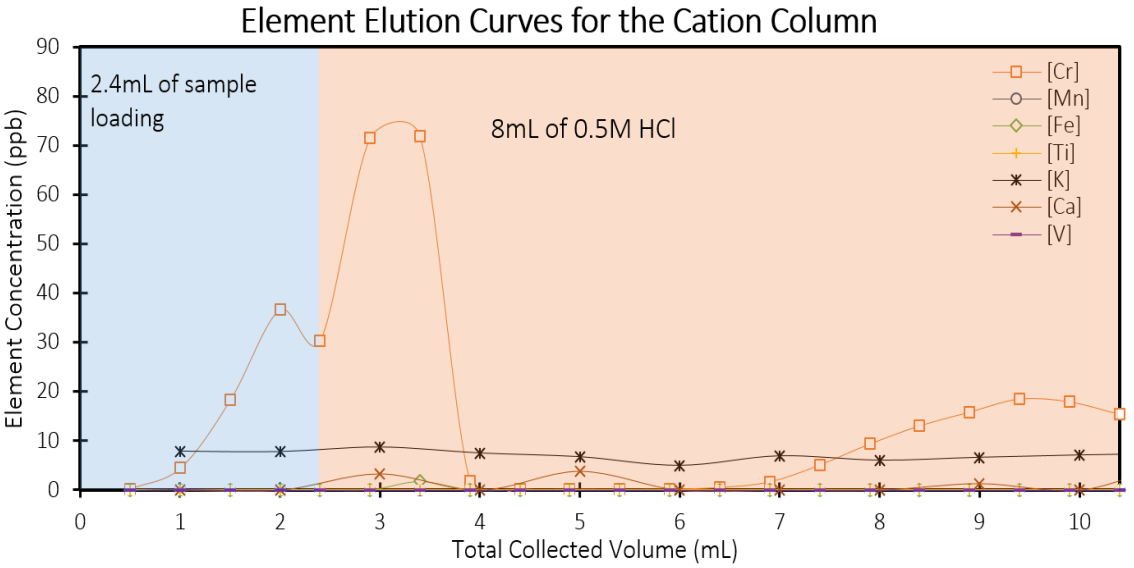

Figure 8. Elemental elution curves of Cr and its interfering elements as well as Ca and K throughout the 'Anion Column' Procedure; where Ca and K represent alkali and alkaline Earth metals, with [Ca] divided by 10 for convenience.

Samples and Reference Materials

In total, 9 samples from the Manbulloo S1 and 18 from the LV09001 drill cores were processed at the University of Adelaide, along with selected standards: BCR-1 (basalt), BHVO-2 (basalt) and JDo-1 (dolomite), normalised to NIST SRM 979 (reference

material). The measured $\delta^{53}Cr$ values for standards analysed at the University of Adelaide are summarised in Table 1 below with their corresponding published values (Table 2 and Figure 10). Furthermore, 20 samples from Manbulloo S1 and 20 more from LV09001 cores were analysed in University of Copenhagen for additional Cr isotope analysis (Figures 11 to 13).

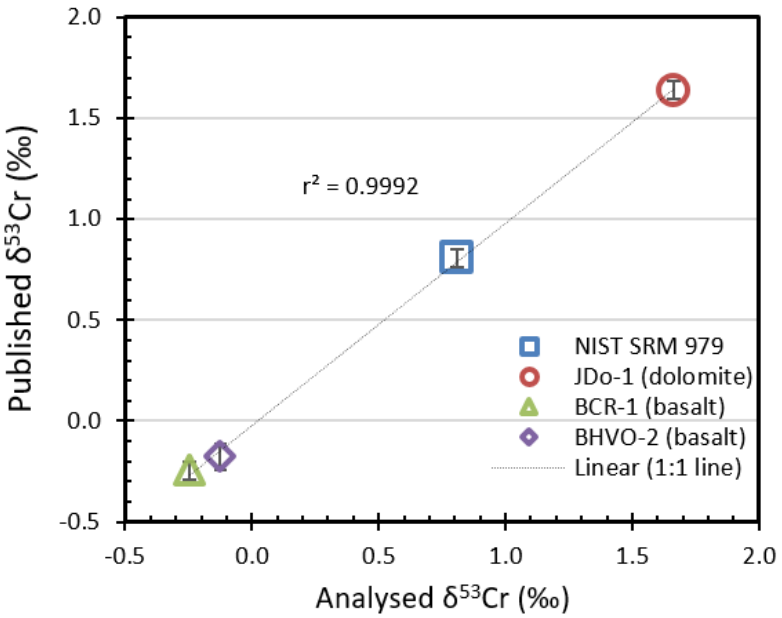

Figure 10. Analysed $\delta^{53}Cr$ values (‰) on standard against published values in Table 2.

Table 1. Standard geological materials analysed for $\delta^{53}Cr$ by TIMS at in the University of Adelaide, using the ^{50}Cr-^{54}Cr DS from Czech Geological Survey (see Farkaš et al. (2013).

Analysis Dates (D/M/Y)	Standards	Cycles	$\delta^{53}Cr \pm 2SE$
1/8/18	JDo-1 (Dolomite)	190	$+1.65 \pm 0.042$
15/8/18	JDo-1 (Dolomite)	200	$+1.60 \pm 0.041$
23/8/18	JDo-1 (Dolomite)	110	$+1.55 \pm 0.054$
23/8/18	JDo-1 (Dolomite)	200	$+1.64 \pm 0.037$
27/8/18	JDo-1 (Dolomite)	100	$+1.64 \pm 0.064$
27/8/18	JDo-1 (Dolomite)	200	$+1.60 \pm 0.037$
17/9/18	JDo-1 (Dolomite)	100	$+1.83 \pm 0.039$
17/9/18	JDo-1 (Dolomite)	200	$+1.79 \pm 0.063$
	Mean JDo-1		$+1.67 \pm 0.047$
	Number of Samples		8
1/8/18	BCR-1 (Basalt)	100	-0.246 ± 0.06
15/8/18	BCR-1 (Basalt)	200	-0.245 ± 0.04
	Mean BCR-1		-0.245 ± 0.045
	Number of Samples		2

17/9/18	BHVO-2 (Basalt)	200	-0.126 ± 0.044
17/9/18	BHVO-2 (Basalt)	200	-0.123 ± 0.086
	Mean BHVO-2		-0.125 ± 0.065
	Number of Samples		2

Table 2. Published δ^{53}Cr values of JDo-1, BCR-1 and BHVO-2, all normalised to NIST SRM 979. Note the lack of minimum samples required for BHVO-2 and BCR-1 bars the calculation of 2SD.

Sample	This Study	(Gilleaudeau et al., 2016)	(Li *et al.*, 2016)	(Schoenberg et al., 2008)
JDo-1	$+1.67$	$+1.64 \pm 0.03$‰	$+1.64 \pm 0.05$‰	----------
BHVO-2	-0.245	----------	-0.155 ± 0.02‰	-0.178 ± 0.05‰
BCR-1	-0.125	No Published Data		

Thermal Ionisation Mass Spectrometry (TIMS) – Cr Isotope Analysis

Samples were loaded on tungsten filaments in a mixture of 1µL of 2N HNO_3 and 1µL of Nb_2O_5 emitter and heated at ~4.0A to evaporate using Isotopx Filament Loading Unit. Insufficient Nb_2O_5 results into poor ionisation, while excessive Nb_2O_5 cause erratic unstable beams likely due to heterogeneous distribution of Nb_2O_5 on the filament (Li et al., 2016). The average blank was estimated at about 10ng (n=4), determined via isotope dilution, using ~80µL of the ^{50}Cr-^{54}Cr DS as a tracer. All Cr isotope measurements in this study were conducted on an Isotopx Phoenix TIMS equipped with six Faraday Collectors (both at University of Adelaide and University of Copenhagen) enabling simultaneous collection of all four Cr beams ($^{50}Cr^+$, $^{52}Cr^+$, $^{53}Cr^+$, $^{54}Cr^+$) together with $^{51}V^+$, and $^{56}Fe^+$ as monitors for potential interference of ^{50}V on ^{50}Cr, and ^{54}Fe on ^{54}Cr. The ^{50}Cr-^{54}Cr DS technique was employed to correct for any mass-dependent Cr isotope fractionation induced either during column chromatography and/or TIMS analysis (i.e. instrumental fractionation).

Data acquisition of Cr isotopes began when the signal intensity of ^{52}Cr reached and maintained at ~1V throughout data acquisition. Each measurement run consists 10 blocks of data with 20 cycles per block. The integration time per cycle was 4 secs. To

eliminate all gain calibration errors, amplifier gains were calibrated at the start of each analytical session. Before analysis, a peak-centre routine was run and then the baseline was measured. The total measuring time per sample, including filament heating, tuning the signal, and collecting data was ~1hr. Corrected Cr isotope data (i.e. $^{53}Cr/^{52}Cr$ sample ratios, or $\delta^{53}Cr$ values) were calculated using double-spiked correction algorithm modified from a similar Zinc DS method published by Samanta, Ellwood, and Mortimer (2016). The correct Cr isotope ratios are expressed by conventional the $\delta^{53}Cr$ notation (Equation 1). NIST SRM 979 was used to monitor the instrument stability over a period of 10 months, utilising ~500ng Cr loads (before column chemistry) with average values of $^{53/52}Cr = 0.000 \pm 0.098$ $(n = 10, 2SD)$.

$$\delta^{53}Cr(‰) = \left(\frac{^{53}Cr/^{52}Cr_{sample}}{^{53}Cr/^{52}Cr_{NIST\ SRM\ 979\ (standard)}} - 1\right) \times 1000$$

Equation 1. Calculation equation delta value, or $\delta^{53}Cr$ normalised to NIST SRM 979 as the standard reference material, see also Frei et al. (2009).

RESULTS

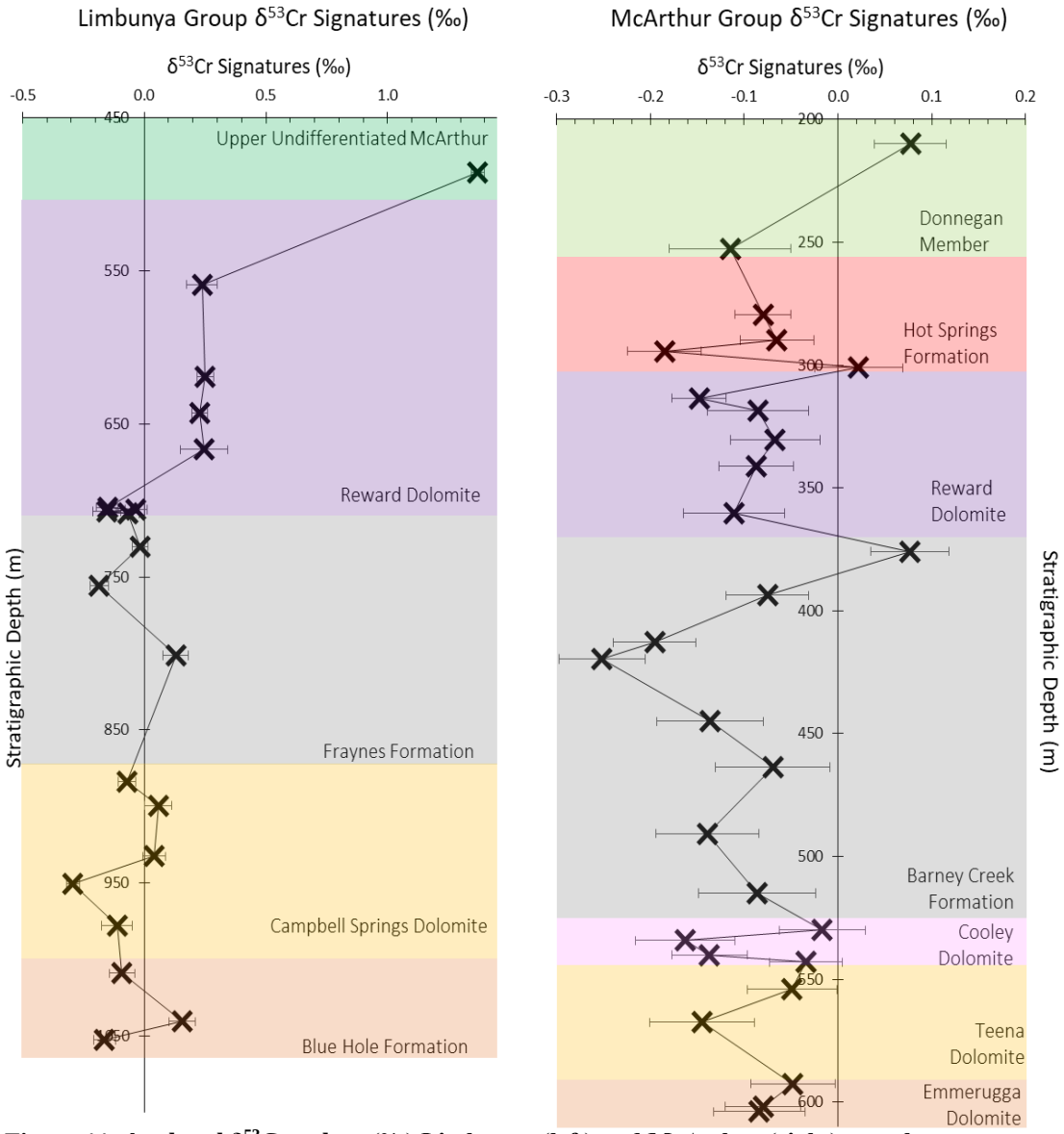

Figure 11. Analysed δ^{53}Cr values (‰) Limbunya (left) and McArthur (right) samples across stratigraphic depth (m) from both University of Adelaide and University of Copenhagen.

A total of 39 (20 from Limbunya and 19 from McArthur Groups) δ^{53}Cr values were successfully analysed and presented in this project. The δ^{53}Cr values analysed from the University of Copenhagen were integrated (i.e. combined) with the data generated from the University of Adelaide. Although similar in age and sedimentology, the Limbunya and McArthur Groups present very different δ^{53}Cr trends over stratigraphic depth

(Figure 11). The δ^{53}Cr values in McArthur Group (Figure 11, right) shows an effectively consistent δ^{53}Cr trend with an average value approaching the crustal signature (i.e. $-0.124‰$). It also shows a rather erratic behaviour of δ^{53}Cr values with some spontaneous changes. Meanwhile, the Limbunya Group (Figure 11, left) presents a more variable spectrum of δ^{53}Cr values with less erratic changes over stratigraphic depth. Over time, there is a noticeably increasing trend with the positive δ^{53}Cr values of the Limbunya Group (i.e. becoming less negative upwards), not observed in the McArthur Group.

The geochemical data of other elements were obtained from Bullen (2017) and Guiliano (2016), analysed using an ICP-MS from the Adelaide Microscopy using a Sr leaching process rather than the utilised 2N HCl.

DISCUSSION

Limbunya and McArthur δ^{53}Cr Values

The similar and coherent δ^{53}Cr and Cr concentration trends between the Adelaide and Copenhagen data in both Limbunya and McArthur Groups (Figures 12 and 13), analysed by almost identical TIMS and double-spiking methods at the two universities, confirm the robustness and suitability of the developed Cr-Purification chromatography, and double-spiking routine, newly established at the University of Adelaide. From this point onwards, the Limbunya Group will be discussed more closely where systematic changes in δ^{53}Cr and Cr concentration have been documented. Any outliers were discarded in any of the correlation calculations.

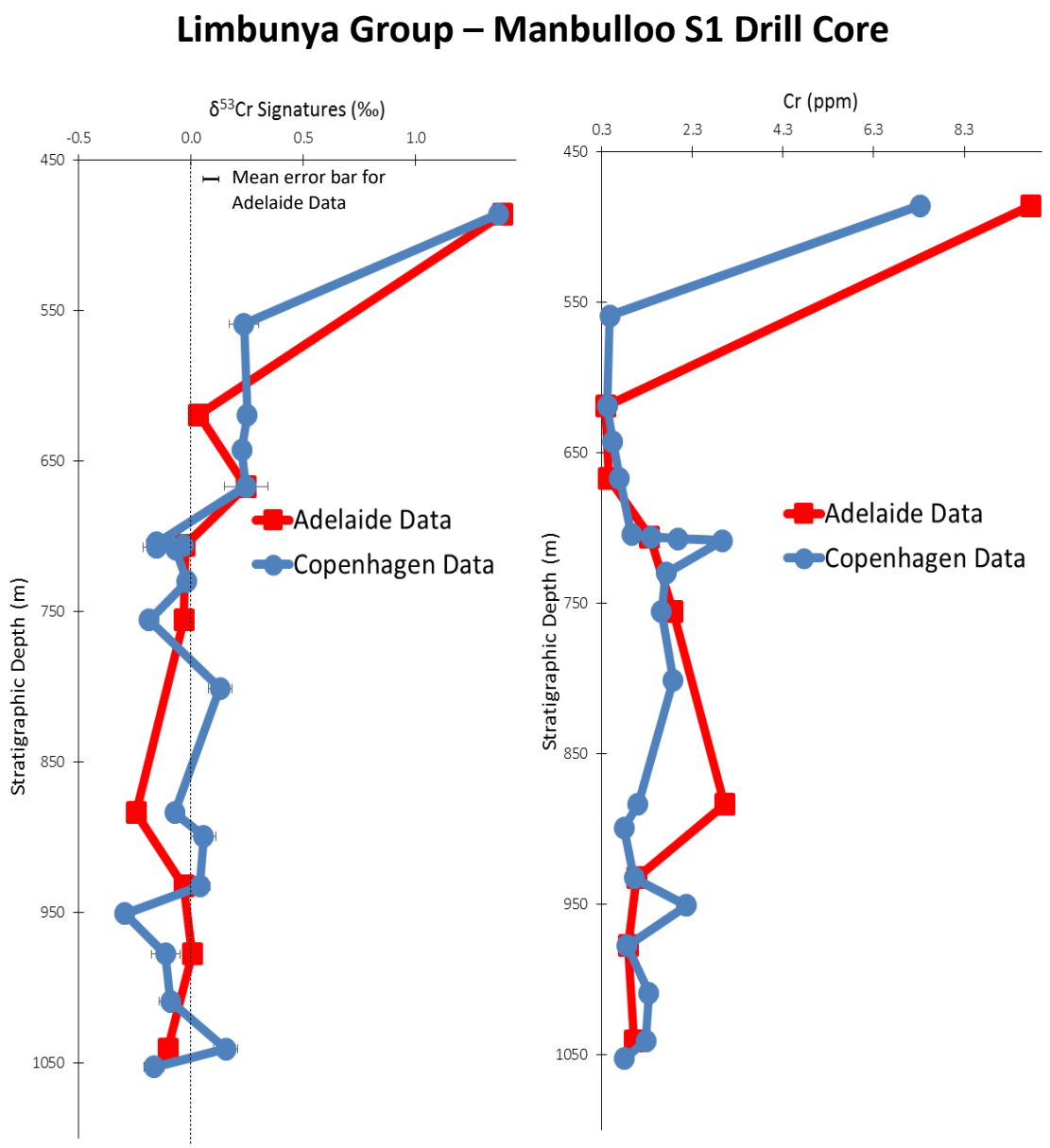

Figure 12. δ^{53}Cr values (‰; left) and Cr (ppm; right) across stratigraphic depth (m) in the Limbunya Group, accessed from Manbulloo S1 drill core. The average error bars of Adelaide data are included due to the enlarged data points.

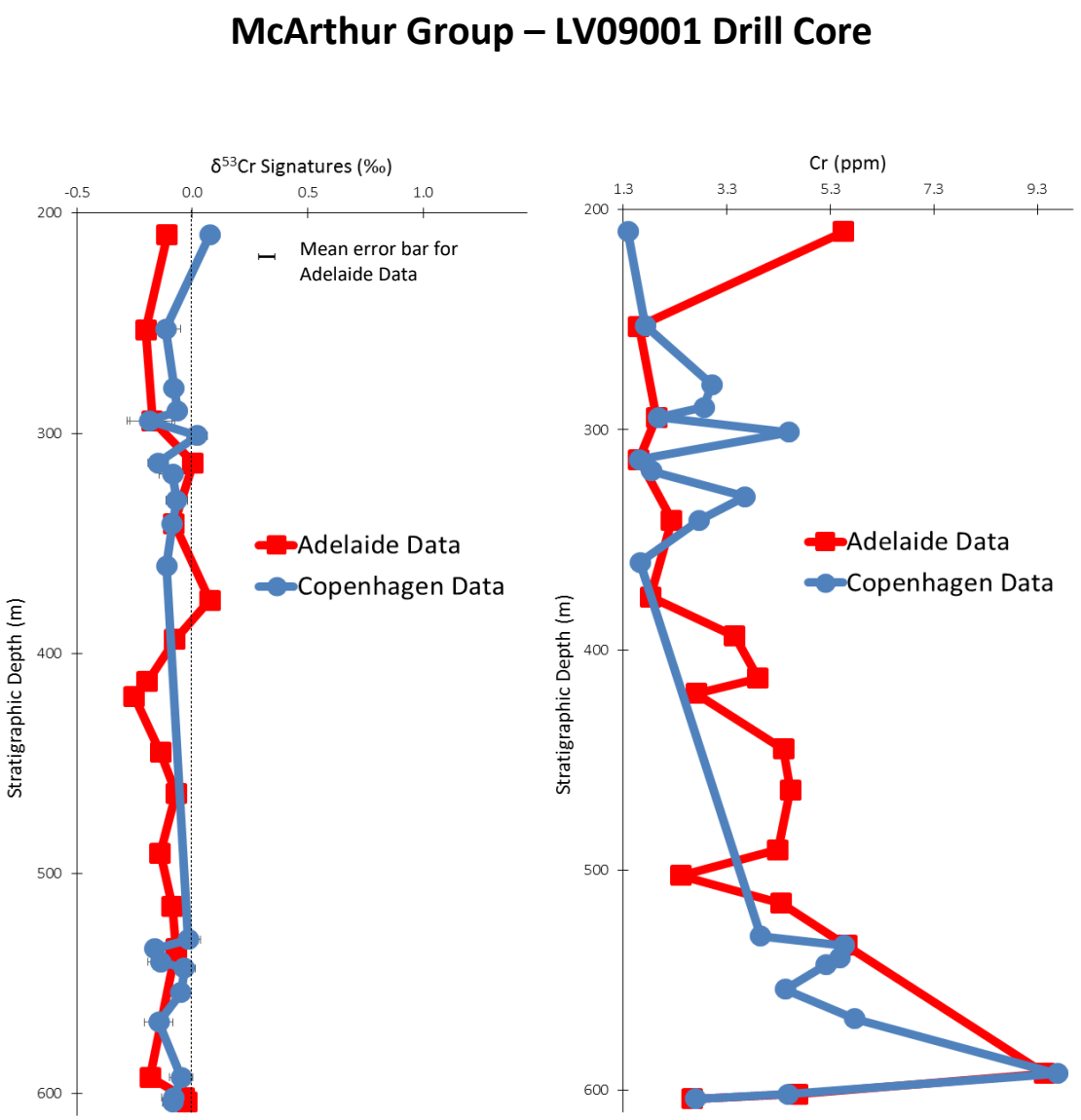

Figure 13. δ^{53}Cr values (‰; left) and Cr (ppm; right) across stratigraphic depth (m) in the McArthur Group, accessed from LV09001 drill core. The average error bars of Adelaide data are included due to the enlarged data points.

A simple hypothetical, yet possibly premature, interpretation to the fluctuating, but increasing, δ^{53}Cr trend in the Limbunya Group (Figures 11 and 12) over stratigraphic depth (older to younger) is a transient release of oxygen over time, possibly either as a commencement of an oxygenation event (global scenario) or as an 'oxygen oasis' via photosynthesising stromatolitic communities (local scenario); should high pO_2 be the dominant causality of these positive δ^{53}Cr, rather than secondary diagenetic processes

caused by later fluid/rock alterations. However, as mentioned, multiple processes can affect Cr isotopes differently, further complicating the above paleo-redox interpretation. Firstly, ligand-complexation fractionation can potentially influence the observed δ^{53}Cr values in these organic-rich facies due to the low energy and restricted settings (Bullen, 2017; Guiliano, 2016), granting ample opportunities for ligand fractionation to occur. Although it is unlikely for this process to dominate the observed δ^{53}Cr values as partial reduction has also been observed to occur as a mechanism that incorporated the Cr into the sediments (Figure 18). The fermentation of organic matter during decomposition might have been the source of organic acids and siderophores, potentially promoting ligand-complexation fractionation of Cr isotopes. Though the effects of ligand-driven fractionation during the Proterozoic Eon (before complex *biota*) remains largely unconstrained (Canfield et al., 2018). As mentioned, its effects on Cr isotopes remain highly uncertain. Hence, future studies should focus more on the causes and effects of organic ligand-complexation fractionation.

Secondly, microbial reduction processes in the water column and/or sediment-water interface could have potentially cause δ^{53}Cr fractionation effects in these samples. The limited δ^{53}Cr fractionations may have predominantly originated from the Cr in these microbes rather than the carbonate and/or shale components, expected to retain more negative δ^{53}Cr. Leaching the organics, carbonates and silicates individually from the samples may resolve this uncertainty; with the most similar δ^{53}Cr values, indicating the source of these observed signals. Additionally, correlating δ^{53}Cr signals with δ^{15}N data from the same samples could be, in future, used an effective method to verify the prominence of microbial activity (e.g. denitrification), as microbial denitrification can

have parallel effects on both $\delta^{53}Cr$ and $\delta^{15}N$ values (Gueguen et al., 2016; Holmden et al., 2016).

Thirdly, kinetics of carbonate formation, may potentially produce isotopic effects during dolomite precipitation, preferentially incorporating either heavy or light Cr isotopes (Farkaš et al., 2018; Pereira *et al.*, 2016; Rodler et al., 2015). These effects are typically inferior relative to Cr isotope effects induced by redox processes

Fourthly, evidence for more positive $\delta^{53}Cr$ values associated with more 'marine' and presumably primitive $^{87}Sr/^{86}Sr$ values in these carbonates are observed (Figure 14). It is more distinctive in the McArthur Group and interpreted to be an already positively fractionated paleo-seawater, and/or local dissolved Cr(VI) pool, being directly incorporated into sediments.

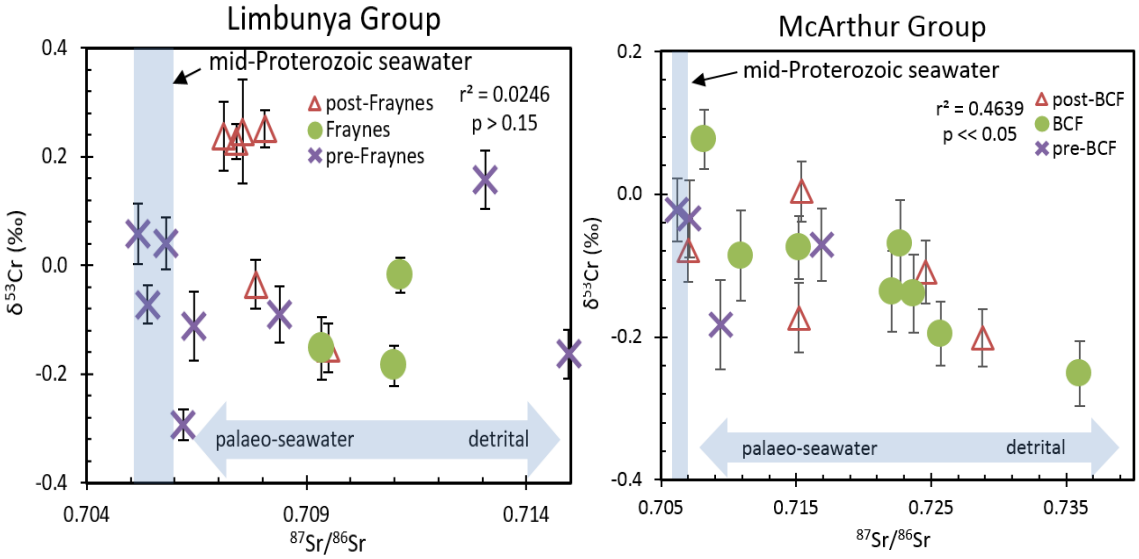

Figure 14. Cross-plots of $^{87}Sr/^{86}Sr$ against $\delta^{53}Cr$ data, where Sr isotopes are used as an index to infer the origins of the observed $\delta^{53}Cr$ values with affinities to either detrital or paleo-seawater Cr sources (see horizontal arrows). BCF indicate samples formed during deposition of Barney Creek Formation, and a vertical rectangle illustrates the expected Sr isotope composition of the coeval paleo-seawater at *ca.* 1.6 Ga (Kuznetsov, Semikhatov, & Gorokhov, 2018). Two more anomalous values with $^{87}Sr/^{86}Sr$ greater than 0.715 were removed to emphasise the argued correlation in the Limbunya Group.

A more likely scenario for the vastly limited $\delta^{53}Cr$ values observed is detrital mixing where $\delta^{53}Cr$ values from lithogenic (i.e. detrital) components dominated the samples as lower Al/Sr ratio and more primitive $^{87}Sr/^{86}Sr$ values (measure of detrital component) is linked with more positive $\delta^{53}Cr$, and *vice versa* where samples with higher Al/Sr and more radiogenic $^{87}Sr/^{86}Sr$ values ratios are associated with more negative $\delta^{53}Cr$ values (Figures 14 and 15). Should these correlations are accurate, it would strongly suggest these $\delta^{53}Cr$ are representative of redox processes and partial reduction of dissolved Cr(VI) in paleo-seawater to Cr(III) (Ellis et al., 2002).

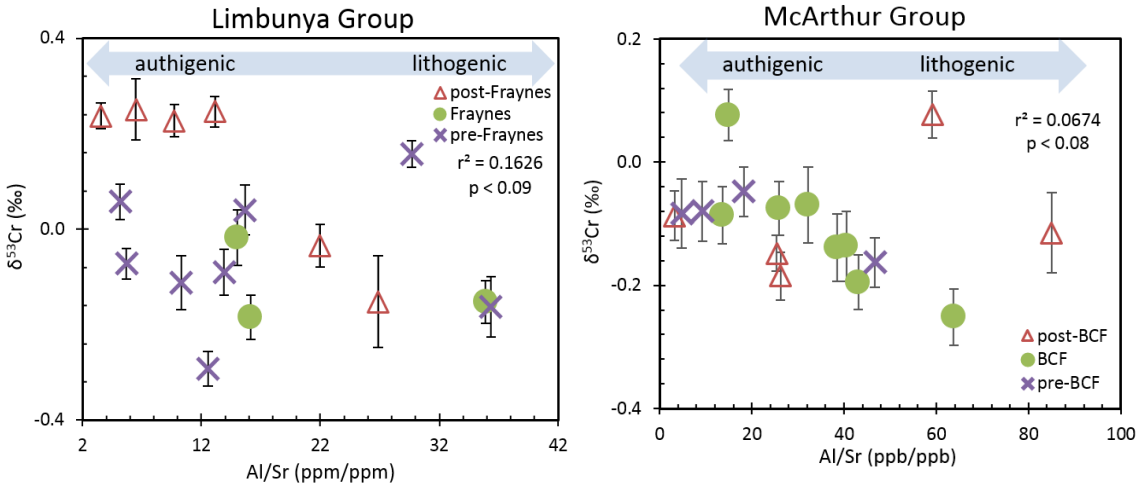

Figure 15. Cross-plots of $\delta^{53}Cr$ data versus Al/Sr ratios in carbonates, where the latter (Al/Sr) is used as an indicator differentiating lithogenic (i.e. detrital) and authigenic (i.e. paleo-seawater) components in analysed samples. BCF = deposition of Barney Creek Formation and two anomalous values with very high Al/Sr were removed to emphasise the argued correlation in the Limbunya Group.

Partial reduction of Cr(VI) by Fe(II)-rich sediments is a possibility that was also weakly observed to occur on these samples; as lower Cr concentrations are correlated with higher $\delta^{53}Cr$ values (Figure 16), which would occur from pools of Cr(VI) under the presence of Fe(II)-rich sediments, proposing that the observed positive values originated from an already fractionated water column, possibly caused by high pO_2, considering multiple values are well above the silicate reservoir range of -0.1‰ to -0.2‰. This

process partially reduces Cr(VI) into Cr(III), simultaneously oxidising Fe(II) to Fe(III), causing Cr isotope fractionation to more positive δ^{53}Cr values as Cr concentrations in the water column decrease (Ellis et al., 2002).

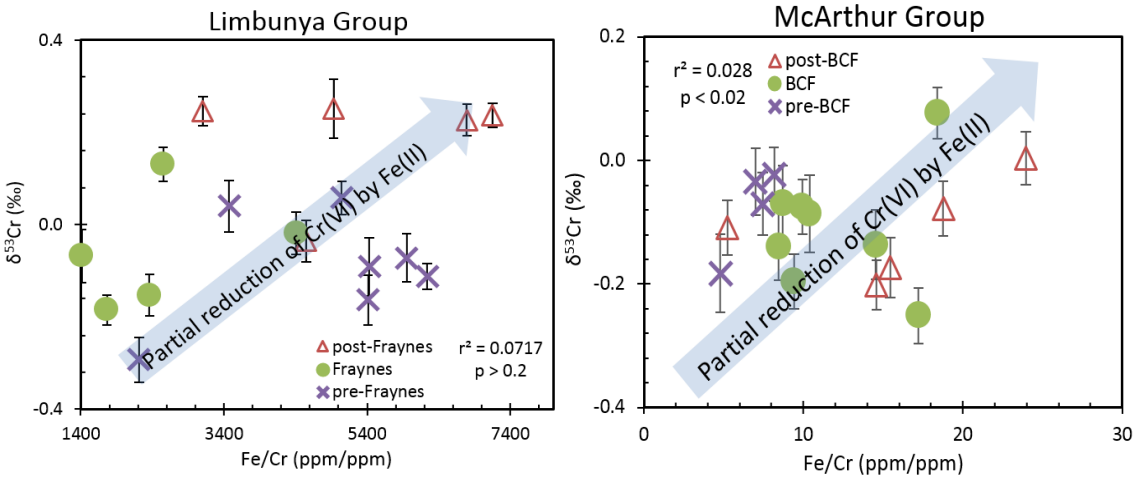

Figure 16. Cross-plots of δ^{53}Cr values versus Fe/Cr ratios, where the latter (i.e. availability of Fe in the system) can be viewed as an indicator for Cr(VI) reduction by Fe(II). Accordingly, higher δ^{53}Cr signatures associated with higher abundances of Fe(II) (or Fe/Cr ratios) suggest higher degree of partial reduction of Cr(VI) reflected by higher δ^{53}Cr values. Anomalous values are disregarded (for details see data in Figure 12 and 13), and two more outliers with higher than 8000 Fe/Cr ratio in the Limbunya Group were removed in an attempt to emphasise the argued correlation.

Moreover, the organic matter in these sediments seemed to greatly influence the more positive δ^{53}Cr values in Limbunya Group as seen in the Figures 11, 12, 14, 15, and 16, when comparing the values pre- and post-Fraynes. The slight, but significant ($p < 0.05$), increase in fractionation with the younger sediments, post-dating deposition of organic-rich shales (i.e. Fraynes Formation), not only provided confidence that atmospheric oxygen is the dominant causality of these positive fractionations, but the governing organisms preserved in these sediments are likely photosynthetic. The intense photosynthetic activity and enhanced biological productivity in the basin is supported by synchronous transition from lower to higher δ^{13}C isotope values during this interval, indicating more biological production in the basin *ca.* 1.64 Ga (Figure 4; (Bullen, 2017).

Now that oxygen levels have been correlated with the positively fractionated $\delta^{53}Cr$ values in the Limbunya Group, it can be postulated that the repetitive fluctuation cycles of $\delta^{53}Cr$ over time (Figures 11 and 12) could possibly be reflective of ancient photosynthetic *biota* attempting to thrive in a harshly reducing environment *ca.* 1.64 billion years ago. Likewise, applying these observations in a global scale would produce an interpretation that such fluctuations are likely reflective of the oscillating exchanges between the sources (e.g. photosynthetic *biota*) and sinks (e.g. H_2S, CH_4, etc.) of atmospheric oxygen during the mid-Proterozoic. This also demonstrates the high sensitivity of Cr isotopes, $\delta^{53}Cr$ as a tracer for paleo-redox conditions. Nevertheless, such interpretations would be premature to exclude the possibility of a bias interpretation. Regarding the highly anomalous value in the upper Limbunya Group, no evidence was found to insinuate it is not representative of redox conditions.

Finally, it is worth mentioning that the McArthur Group, especially the Barney Creek Formation, is very likely to suffer from late diagenetic effects as Baruch et al. (2015) mentioned that the BCF experienced substantial amounts of diagenetic alteration (i.e. silicified formations). Although the effects of diagenetic alteration on Cr isotopes is completely unconstrained, Canfield et al. (2018) mentioned that it may alter the $\delta^{53}Cr$ and Cr concentrations during diagenesis, summarising that the BCF and, to a lesser extent, the McArthur Group may not be the most ideal units to measure $\delta^{53}Cr$ values on, unrepresentative of the paleo-redox conditions. Correspondingly, such diagenetic alteration effects may have caused the limited $\delta^{53}Cr$ observed in the McArthur Group, resetting the distribution of Cr isotopic masses, resulting to the observed $\delta^{53}Cr$ values approaching near crustal values. The minimal fluctuations in the McArthur $\delta^{53}Cr$ values could possibly be an effect of the fluid infill event on Cr isotope values. Considering

that most of the McArthur units analysed have been greatly influenced by a Si-rich infill, connotes the possibility of the observed non-fractionated Cr isotopes values being more representative of the Si-rich fluid, systematically masking the paleo-redox signals to generally anoxic conditions (Holmden et al., 2016). Such a scenario is very possible as hydrothermal fluids can largely contain δ^{53}Cr values approaching the crustal values (i.e. -0.124‰; (Holmden et al., 2016).

Additionally, Mukherjee and Large (2017) found strong evidence of exhalative hydrothermal alteration of the BCF from trace element analysis on pyrite, even emphasising indications that most paleo-redox tracers, expect for Se and Bi, would be ineffective and would present interpretations unrepresentative of paleo-redox conditions (Figure 17). Although Mukherjee and Large (2017) did not specifically mention Cr as an ineffective paleo-redox tracer for the BCF, these findings could be evidence to suggest Cr isotope values from the McArthur Group, are systematically altered by hydrothermal influences, since the LV09001 core is proximal to the HYC ore deposit (<50 km apart). If genuine, the model for a commencement of global oxygenation event *ca.* 1.64 Ga remains as a plausible occurrence.

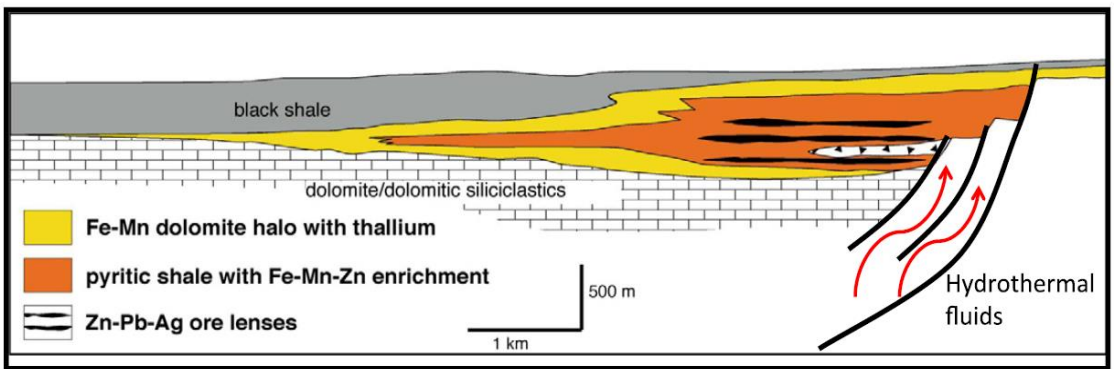

Figure 17. Demonstrative diagram of the intense exhalative hydorthermal alteration that pervaded the Barney Creek Formation (Mukherjee and Large, 2016), likely resetting δ^{53}Cr values to near crustal values (i.e. -0.124‰), resulting to the near-constant values observed in this study.

Rayleigh Models for Coupled δ^{53}Cr and Cr Concentration Trends in Carbonates

The following section attempts to model the paleo-redox processes in the Proterozoic seawater and their expected effects on both δ^{53}Cr and Cr concentration data recorded in these marine carbonates. Three possible Rayleigh fractionation models, adopted from Ellis et al. (2002), Farkaš et al. (2013) and Farkaš et al. (2018), were constructed to simulate variations in δ^{53}Cr and Cr concentration data in Limbunya Group carbonates (Figure 18) in an attempt to quantify the trends observed. The model proposes that the true instantaneous Cr isotope fractionation factor, α, between Cr(VI) to Cr(III) species for the samples lies somewhere between 0.9997 and 0.99995. The result of these Rayleigh Fractionation models is calculation of the expected δ^{53}Cr value of the remaining dissolved hexavalent Cr(VI) pool in the paleo-seawater as a function of the continuous removal (i.e. reduction) of Cr(VI) into insoluble Cr(III), reflected by the 'fraction' or *f* parameter in the model, which varies between 0 and 1 (Equation 2; Ellis et al., 2002). In this study, the *f* is normalised from the Cr concentrations of the samples. Although the resulting fractionation model is far from perfect, it is adequate to explain and correlate some of the variability seen in the data.

$$\delta^{53}Cr = [(\delta^{53}Cr_{initial} + 10^3)f^{\alpha-1}] - 10^3$$

Equation 2. Rayleigh Fractionation equation to calculate the Cr isotope composition (δ^{53}Cr) of remaining and partially reduced Cr(VI), using value of α or isotope fractionation factor associated with reduction of Cr(VI) to Cr(III). Note that the δ^{53}Cr represents the Cr isotope signature of Cr(VI) in seawater, as a function of f or the fraction of remaining unreacted hexavalent Cr(VI) pool (Ellis et al., 2002). $\delta^{53}Cr_{initial}$ represents the initial Cr isotope composition of paleo-seawater or unreacted Cr(VI) pool in McArthur Basin at ca. 1.64 Ga, in our model corresponding to the lowest analysed δ^{53}Cr value of -0.29‰.

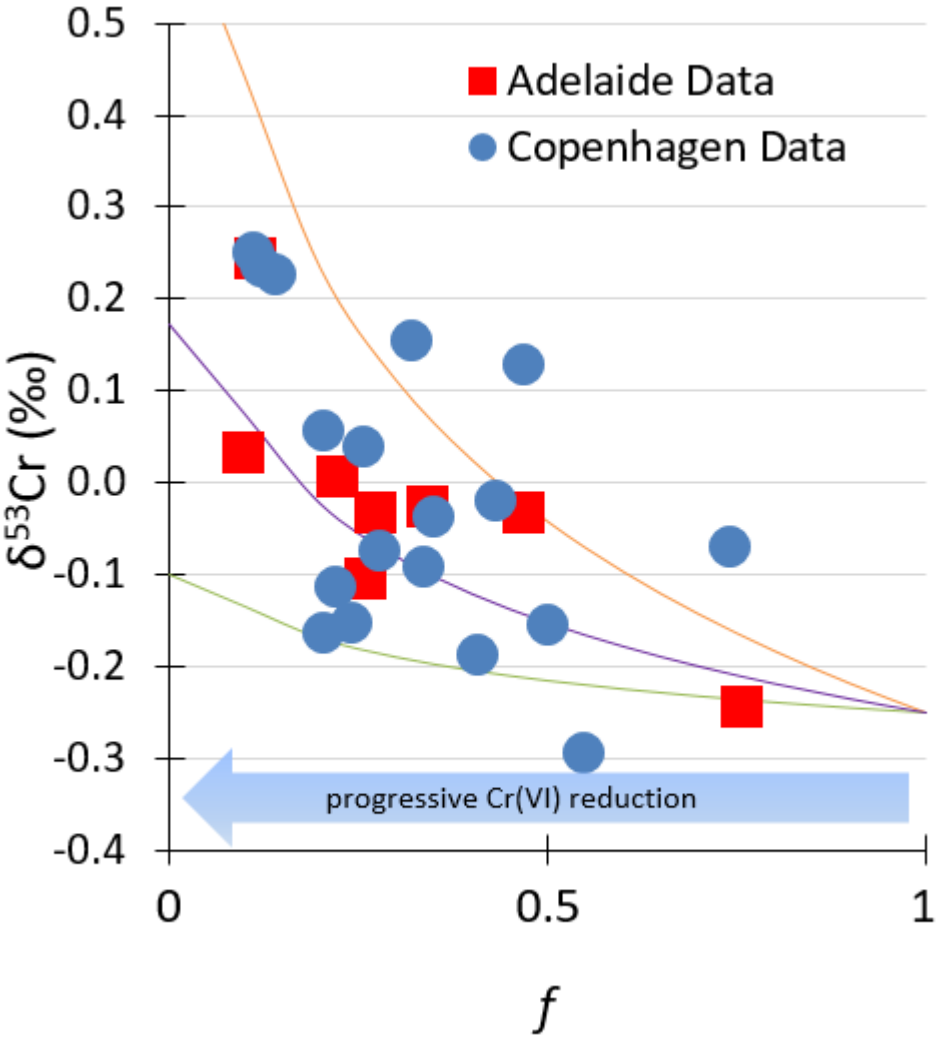

Figure 18. Rayleigh fractionation model for the $\delta^{53}Cr$ to simulate data from the Limbunya Group, as a function of *f* or partial reduction and removal of Cr(VI) from seawater. Top line, $\alpha = 0.99995$; middle line, $\alpha = 0.999859$; and bottom line, $\alpha = 0.9997$ best-fitting curves for the Limbunya Group. *f* means fraction of the remaining unreacted Cr(VI), normalised from Cr concentration (ppm).

Interpretation Overview

In summary, the positively fractionated $\delta^{53}Cr$ values feasibly originated from an already positively fractionated paleo-seawater (primitive $^{87}Sr/^{86}Sr$; Figure 14) where more lithogenic components (high Al/Sr) likely dominated the more negative $\delta^{53}Cr$ values (Figure 15). There are evidence to suggest exhalative hydrothermal influences on the $\delta^{53}Cr$ values in the McArthur Group, especially the BCF, rendering any Cr isotope data

to be unrepresentative of paleo-redox conditions while the $\delta^{53}Cr$ values in the Limbunya are more representative of the paleo-redox conditions. Although not clearly observed, Cr(VI) reduction via Fe(II)-rich sediments likely played a role in reducing Cr(VI) into these sediments (Figure 16). Carbonate precipitation and biomineralisation are also possible processes that integrated authigenic $\delta^{53}Cr$ signals into these rocks.

Two possible scenarios have been proposed for the vastly differing $\delta^{53}Cr$ values between the Limbunya and McArthur Groups. The less likely scenario to have occurred is that all $\delta^{53}Cr$ values from both groups are representative of paleo-redox conditions where the more variable $\delta^{53}Cr$ values in the Limbunya Group insinuate a gradual increase of atmospheric pO_2, possibly caused by a local oxygen oasis; and the consistent $\delta^{53}Cr$ values in the McArthur Group indicate a more reducing local environment at the time. Conversely, a more feasible scenario to occur is that $\delta^{53}Cr$ values in the McArthur Group have been reset by a nearby exhalative hydrothermal alteration, expected to produce more negative $\delta^{53}Cr$ values, unrepresentative of paleo-redox conditions. Whereas, the $\delta^{53}Cr$ values in the Limbunya Group is more representative of paleo-redox conditions, suggestive of the minor fluctuations of pO_2 occurring at the time, possibly rising gradually as a commencement of an oxygenation event. These interpretations are under the heavy assumption that pO_2 is the predominant causality of this positively fractionated paleo-seawater and, detrital and organic materials be the overriding source of the limited $\delta^{53}Cr$ fractionations. A schematic diagram for the summarised interpreted scenarios are presented (see Figure 19).

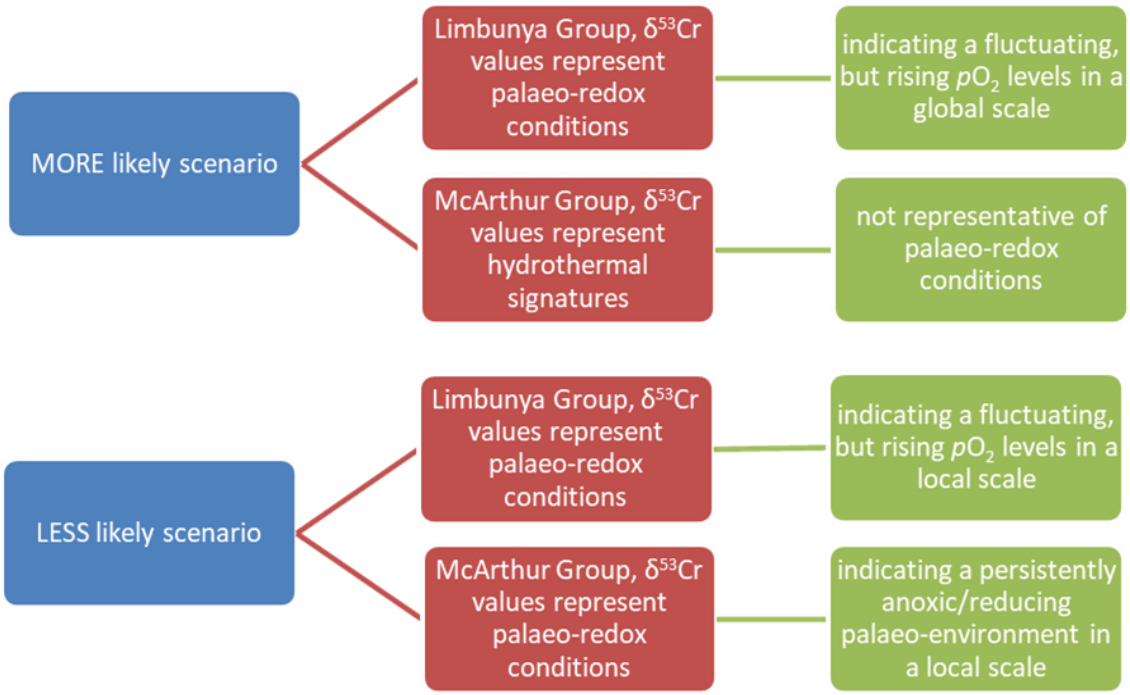

Figure 19. Schematic diagram presenting the simplified possible scenarios postulated based on the δ^{53}Cr data from both Limbunya and McArthur Groups.

Implications of the oldest positively fractionated Cr in marine carbonates for biological evolution

A local-scale oxygenation would require a mechanism that hypersaturates the local marine environment with dissolved O_2 before being released into the atmosphere. Such mechanism would be consistent with current knowledge of the Paleoproterozoic *biota*, under the common assumption that effectively all photosynthetic life at the time are marine/aquatic. Conversely, a global-scale oxidative terrestrial weathering would likely produce more parallel δ^{53}Cr fractionation patterns between the two groups, supporting a high pO_2 model, possibly providing permissive environment to promote *Eukarya* diversification during the mid-Proterozoic. If genuine, these findings would denote multiple and possibly transient, oxygenation events punctuating the oxygen-depleted mid-Proterozoic time period.

Collectively with the Canfield et al. (2018), Cole et al. (2016), Cox et al. (2016), Diamond et al. (2018), Gilleaudeau et al. (2016), Hardisty et al. (2017), Kendall et al.

(2009), Planavsky et al. (2014), Sheen et al. (2018), Tang et al. (2016), S. Yang et al. (2017), and Zhang et al. (2016) studies, a more feasible scenario is that atmospheric oxygen during the mid-Proterozoic was neither persistently low nor constantly high (Figures 20 and 21), but experienced a more transient and periodic release of O_2 over time. Such a phenomena would produce a highly unstable environment during the mid-Proterozoic, possibly inhibiting *biota* diversification, should atmospheric oxygen levels truly be a barrier for *Eukarya* evolution, as asserted by geoscientists. Contrariwise, a more likely scenario is that *Eukarya* evolution was not solely constrained by oxygen levels, but rather with other limiting trace nutrients essential for life, such as Se, Ni, Cu, Co, Mo, Zn, Cd, P, etc. (Cox *et al.*, 2018; Mukherjee *et al.*, 2018). This phenomena would situate high pO_2 being the effect of biological evolution rather than its causality (Butterfield, 2009, 2018; Charles W. Diamond & Lyons, 2018). The two possible transient oxygenation events recently discovered at *ca.* 1.4 Ga (Canfield et al., 2018; Cox et al., 2016; S. Yang et al., 2017; Zhang et al., 2016) and, at *ca.* 1.1 Ga (Gilleaudeau et al., 2016; Sheen et al., 2018); already hint the possibility of a more complex understanding of the mid-Proterozoic redox conditions (Figures 20 and 21). Mukherjee et al. (2018) found very strong evidence that trace nutrient elements were very scarce in the mid-Proterozoic oceans, which applied immense stress onto the oxygen-deprived *biota*, forcing a prokaryote to adapt by consuming another; eventually becoming the first eukaryote organism. Such a mechanism did not require substantial amounts of oxygen to occur, supporting a more modern view that high pO_2 was unnecessary to promote evolution. Similarly, Cox et al. (2018) found equally robust evidence of phosphorus availability, as a limiting nutrient, to be strongly correlated with the increase of pO_2, as it is being transported from the cooling mantle to the oceans via

weathering; again, providing evidence of an 'oxygen-deprived evolution' where high O_2 levels could likely be an effect, rather than a cause of ancient *biota* evolution (Butterfield, 2009, 2018; Diamond & Lyons, 2018). Hence, the current view of atmospheric oxygen being a barrier for evolution may need to be revised for more modern perspectives.

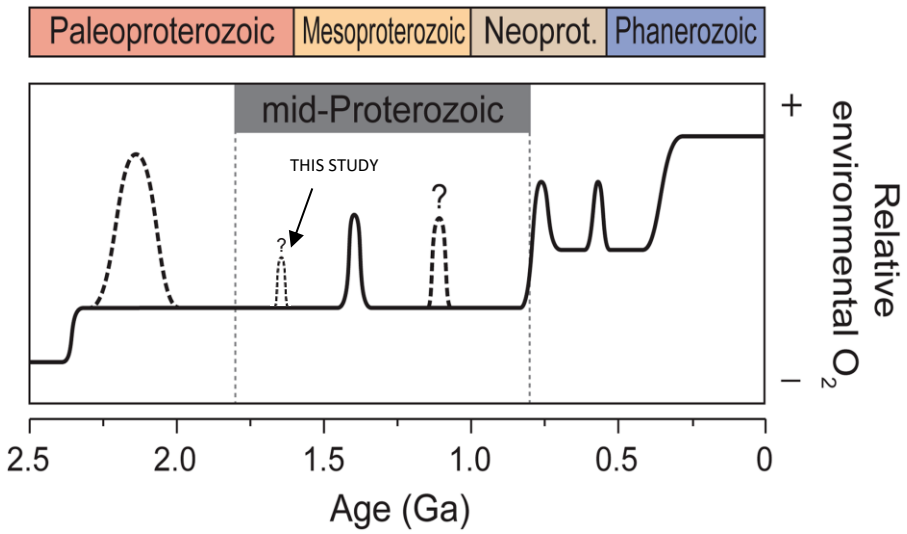

Figure 20. Relative oxygen levels over geological time (Ga) emphasising the two recently discovered possible transient oxygenation events (*ca.* 1.4 and 1.1 Ga) during the mid-Proterozoic. To a lesser extent, it also includes a possible commencement of oxygenation event or an 'oxygen oasis' at *ca.* 1.64 Ga (this study), adapted from Diamond *et al.* (2018).

Nonetheless a higher resolution Cr isotope of data from global Proterozoic marine record is required, not only to understand the redox conditions of the paleo-atmosphere, but also to better understand the more local processes that affect Cr isotopes. A more efficient carbonate leaching treatment (e.g. using 0.5N HCl or acetic acid) is also recommended to minimise the effects of detrital contamination and increase probability to obtain primary $\delta^{53}Cr$ values more representative of past redox conditions.

CONCLUSIONS

The Cr isotope biogeochemistry applied to paleo-studies is still in its foetal stages and future detail and more systematic work is needed to make such a novel isotope proxy a

robust tracer for paleo-redox conditions on the Earth's surface, including the ocean-atmosphere system. Although most of the Cr isotope data acquired by this study insinuate predominantly reducing or low pO_2 conditions at *ca.* 1.64 Ga, there are also some evidence to support a commencement of a possible rise in pO_2 during the mid-Proterozoic. If genuine, this study also reports the oldest positively fractionated $\delta^{53}Cr$ values in the mid-Proterozoic *ca.* 1.64 billion years ago. It is likely that the stagnant diversification of *Eukarya* during the mid-Proterozoic is caused by either high atmospheric oxygen instability in the same time period (Figures 20 and 21) or, alternatively, the scarcity of limiting bio-essential nutrients; or a combination of both.

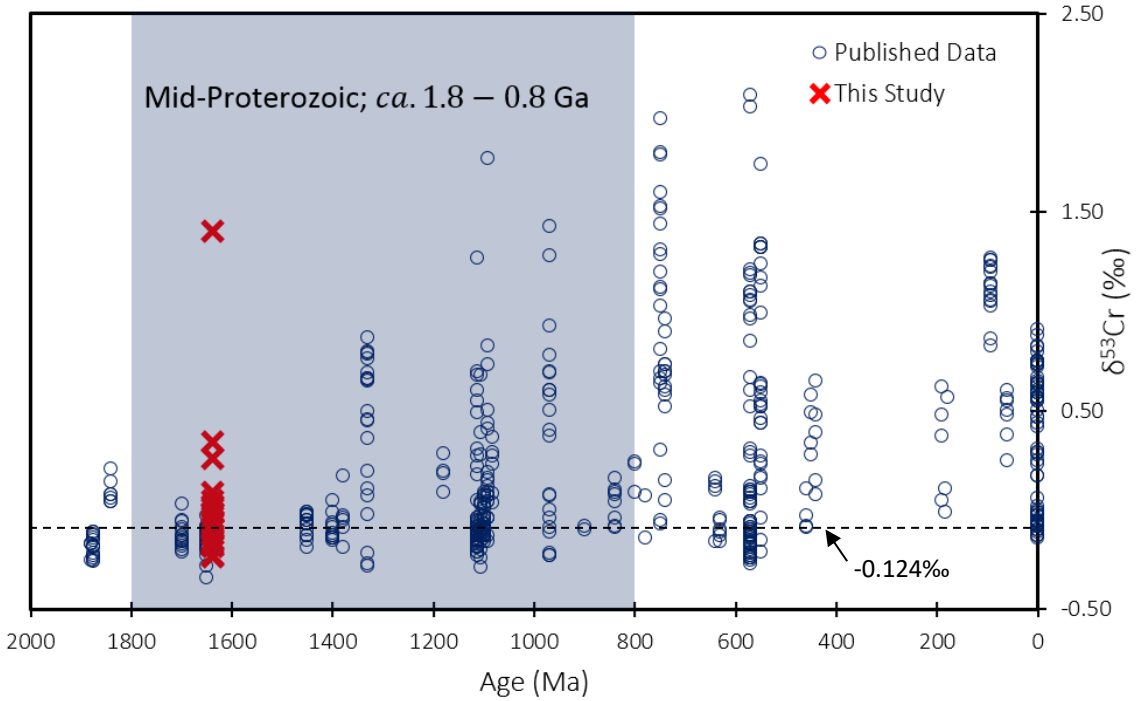

Figure 21. Published Cr isotope record, $\delta^{53}Cr$ (‰), of marine sediments over Geologic Time (Ma) compared to this study (Canfield *et al.*, 2018; Cole *et al.*, 2016; Frei *et al.*, 2016; Frei *et al.*, 2009; Gilleaudeau *et al.*, 2016; Gueguen *et al.*, 2016; Planavsky *et al.*, 2014).

ACKNOWLEDGMENTS

I would like to acknowledge the efforts of everyone who helped me made this project successful. First and foremost, I would like to acknowledge and deeply appreciate the help and guidance of **Dr Juraj Farkaš**, my supervisor who made this quality project accomplishable as well as the imperative academic advice. A great deal of thanks to **Dr Robert Klaebe** and **David Bruce** who I constantly bombarded with questions and advice, which is a colossal part of this project. Another thanks to **Dr Grant Cox** and **Dr Moneesha Samanta** who had to deal with my constant annoyances and provided me with fundamental knowledge and laboratory skills needed, also a major part of this project as well as to **Professor Alan Collins** for making the **ARC Linkage Project** possible, which is a collaboration of *Northern Territory Geological Survey*, *Santos*, *University of Adelaide*, *Origin and Australian Research Council* that provided the funding needed to start and finish this project. I acknowledge the moral support of the **2018 Geology Honours cohort**, including **Dr Alec Walsh**. Lastly, I appreciate the efforts of **Liam Scarabotti** who helped me in learning the chromatography and the **Frei Group** in the University of Copenhagen for the additional Cr analysis. I bid them best of luck in the future.

REFERENCES

BARUCH, E. T., KENNEDY, M. J., LÖHR, S. C., & DEWHURST, D. N. (2015). Feldspar dissolution-enhanced porosity in Paleoproterozoic shale reservoir facies from the Barney Creek Formation (McArthur Basin, Australia). *AAPG Bulletin, 99*(09), 1745-1770. doi: 10.1306/04061514181

BEKKER, A., HOLLAND, H. D., WANG, P.-L., III, D. R., STEIN, H. J., HANNAH, J. L., . . . BEUKES, N. J. (2004). Dating the rise of atmospheric oxygen. *Nature, 427*, 5.

BULLEN, M. (2017). *Isotopic Constraints on the Depositional Environment and Paleo-Redox Conditions of the Greater McArthur Basin, Northern Territory.* (Honours), University of Adelaide, The University of Adelaide.

BUTTERFIELD, N. J. (2009). Oxygen, animals and oceanic ventilation: an alternative view. *Geobiology, 7*(1), 1-7. doi: 10.1111/j.1472-4669.2009.00188.x

BUTTERFIELD, N. J. (2018). Oxygen, animals and aquatic bioturbation: An updated account. *Geobiology, 16*(1), 3-16. doi: 10.1111/gbi.12267

CANFIELD, D. E., ZHANG, S., FRANK, A. B., WANG, X., WANG, H., SU, J., . . . FREI, R. (2018). Highly fractionated chromium isotopes in Mesoproterozoic-aged shales and atmospheric oxygen. *Nat Commun, 9*(1), 2871. doi: 10.1038/s41467-018-05263-9

COLE, D. B., REINHARD, C. T., WANG, X., B., G., HALVERSON, G. P., GIBSON, T., . . . PLANAVSKY, N. J. (2016). A shale-hosted Cr isotope record of low atmospheric oxygen. *Geology, 44*(7), 555-558. doi: 10.1130/G37787.1

COX, G. M., JARRETT, A., EDWARDS, D., CROCKFORD, P. W., HALVERSON, G. P., COLLINS, A. S., . . . LI, Z.-X. (2016). Basin redox and primary productivity within the Mesoproterozoic Roper Seaway. *Chemical Geology, 440*, 101-114. doi: 10.1016/j.chemgeo.2016.06.025

COX, G. M., LYONS, T. W., MITCHELL, R. N., HASTEROK, D., & GARD, M. (2018). Linking the rise of atmospheric oxygen to growth in the continental phosphorus inventory. *Earth and Planetary Science Letters, 489*, 28-36. doi: 10.1016/j.epsl.2018.02.016

DIAMOND, C. W., & LYONS, T. W. (2018). Mid-Proterozoic redox evolution and the possibility of transient oxygenation events. *Emerging Topics in Life Sciences, 2*(2), 235-245. doi: 10.1042/etls20170146

DIAMOND, C. W., PLANAVSKY, N. J., WANG, C., & LYONS, T. W. (2018). What the ~1.4 Ga Xiamaling Formation can and cannot tell us about the mid-Proterozoic ocean. *Geobiology, 16*(3), 219-236. doi: 10.1111/gbi.12282

ELLIS, A. S., JOHNSON, T. M., & BULLEN, T. D. (2002). Chromium Isotopes and the Fate of Hexavalent Chromium. *Science, 295*(5562), 2060-2062. doi: 10.1126/science.1068368

FARKAŠ, J., CHRASTNÝ, V., NOVÁK, M., ČADKOVA, E., PAŠAVA, J., CHAKRABARTI, R., . . . BULLEN, T. D. (2013). Chromium isotope variations (δ53/52Cr) in mantle-derived sources and their weathering products: Implications for environmental studies and the evolution of δ53/52Cr in the Earth's mantle over geologic time. *Geochimica et Cosmochimica Acta, 123*, 74-92. doi: 10.1016/j.gca.2013.08.016

FARKAŠ, J., FRÝDA, J., PAULUKAT, C., HATHORNE, E. C., MATOUŠKOVÁ, Š., ROHOVEC, J., . . . FREI, R. (2018). Chromium isotope fractionation between modern seawater and biogenic carbonates from the Great Barrier Reef, Australia: Implications for the paleo-seawater δ 53 Cr reconstruction. *Earth and Planetary Science Letters, 498*, 140-151. doi: 10.1016/j.epsl.2018.06.032

FREI, R., CROWE, S. A., BAU, M., POLAT, A., FOWLE, D. A., & DOSSING, L. N. (2016). Oxidative elemental cycling under the low O2 Eoarchean atmosphere. *Sci Rep, 6*, 21058. doi: 10.1038/srep21058

FREI, R., GAUCHER, C., POULTON, S. W., & CANFIELD, D. E. (2009). Fluctuations in Precambrian atmospheric oxygenation recorded by chromium isotopes. *Nature, 461*(7261), 250-253. doi: 10.1038/nature08266

FREI, R., POIRÉ, D., & FREI, K. M. (2014). Weathering on land and transport of chromium to the ocean in a subtropical region (Misiones, NW Argentina): A chromium stable isotope perspective. *Chemical Geology, 381*, 110-124. doi: 10.1016/j.chemgeo.2014.05.015

GILLEAUDEAU, G. J., FREI, R., KAUFMAN, A. J., KAH, L. C., AZMY, K., BARTLEY, J. K., . . . KNOLL, A. H. (2016). Oxygenation of the mid-Proterozoic atmosphere: clues from chromium isotopes in carbonates. *Geochemical Perspectives Letters*, 178-187. doi: 10.7185/geochemlet.1618

GRAHAM, A. M., & BOUWER, E. J. (2010). Rates of Hexavalent Chromium Reduction in Anoxic Estuarine Sediments: pH Effects and the Role of Acid Volatile Sulfides. *Environ. Sci. Technol., 44*, 7.

GUEGUEN, B., REINHARD, C. T., ALGEO, T. J., PETERSON, L. C., NIELSEN, S. G., WANG, X., . . . PLANAVSKY, N. J. (2016). The chromium isotope composition of reducing and oxic marine sediments. *Geochimica et Cosmochimica Acta, 184*, 1-19. doi: 10.1016/j.gca.2016.04.004

GUILIANO, W. C. (2016). *Isotope Constraints on Paleo-Depositional Environments and Intra-Basin Correlation in the Proterozoic McArthur Basin, Northern Territory, Australia.* (Honours), University of Adeliade, Adelaide.

HARDISTY, D. S., LU, Z., BEKKER, A., DIAMOND, C. W., GILL, B. C., JIANG, G., . . . LYONS, T. W. (2017). Perspectives on Proterozoic surface ocean redox from iodine contents in ancient and recent carbonate. *Earth and Planetary Science Letters, 463*, 159-170. doi: 10.1016/j.epsl.2017.01.032

HOLLAND, H. D. (2006). The oxygenation of the atmosphere and oceans. *Philos Trans R Soc Lond B Biol Sci, 361*(1470), 903-915. doi: 10.1098/rstb.2006.1838

HOLMDEN, C., JACOBSON, A. D., SAGEMAN, B. B., & HURTGEN, M. T. (2016). Response of the Cr isotope proxy to Cretaceous Ocean Anoxic Event 2 in a pelagic carbonate succession from the Western Interior Seaway. *Geochimica et Cosmochimica Acta, 186*, 277-295. doi: 10.1016/j.gca.2016.04.039

KENDALL, B., CREASER, R. A., GORDON, G. W., & ANBAR, A. D. (2009). Re–Os and Mo isotope systematics of black shales from the Middle Proterozoic Velkerri and Wollogorang Formations, McArthur Basin, northern Australia. *Geochimica et Cosmochimica Acta, 73*(9), 2534-2558. doi: 10.1016/j.gca.2009.02.013

KUZNETSOV, A. B., SEMIKHATOV, M. A., & GOROKHOV, I. M. (2018). Strontium Isotope Stratigraphy: Principles and State of the Art. *Stratigraphy and Geological Correlation, 26*(4), 367-386. doi: 10.1134/s0869593818040056

LAMB, D. M., AWRAMIK, S. M., CHAPMAN, D. J., & ZHU, S. (2009). Evidence for eukaryotic diversification in the ~1800 million-year-old Changzhougou Formation, North China. *Precambrian Research, 173*(1-4), 93-104. doi: 10.1016/j.precamres.2009.05.005

LI, C.-F., FENG, L.-J., WANG, X.-C., CHU, Z.-Y., GUO, J.-H., & WILDE, S. A. (2016). Precise measurement of Cr isotope ratios using a highly sensitive Nb2O5 emitter by thermal ionization mass spectrometry and an improved procedure for separating Cr from geological materials. *Journal of Analytical Atomic Spectrometry, 31*(12), 2375-2383. doi: 10.1039/c6ja00265j

LYONS, T. W., REINHARD, C. T., & PLANAVSKY, N. J. (2014). The rise of oxygen in Earth's early ocean and atmosphere. *Nature, 506*(7488), 307-315. doi: 10.1038/nature13068

MOOS, S. B. (2018). *The Marine Biogeochemistry pf Chromium Isotopes.* (Doctor of Philisophy), Massachusets Institute of Technology, Massachusetts.

MUKHERJEE, I., & LARGE, R. (2017). Application of pyrite trace element chemistry to exploration for SEDEX style Zn-Pb deposits: McArthur Basin, Northern Territory, Australia. *Ore Geology Reviews, 81*, 1249-1270. doi: 10.1016/j.oregeorev.2016.08.004

MUKHERJEE, I., LARGE, R. R., CORKREY, R., & DANYUSHEVSKY, L. V. (2018). The Boring Billion, a slingshot for Complex Life on Earth. *Sci Rep, 8*(1), 4432. doi: 10.1038/s41598-018-22695-x

PAULUKAT, C. (2016). *Chromium stable isotope fractionation in modern biogeochemical cycling: Insights from continental weathering flux to the ocean, and chromium incorporation into carbonate shells.* (Ph.D), University of Copehagen.

PEREIRA, N. S., VOEGELIN, A. R., PAULUKAT, C., SIAL, A. N., FERREIRA, V. P., & FREI, R. (2016). Chromium-isotope signatures in scleractinian corals from the Rocas Atoll, Tropical South Atlantic. *Geobiology, 14*(1), 54-67. doi: 10.1111/gbi.12155

PLANAVSKY, N. J., REINHARD, C. T., WANG, X., THOMSON, D., MCGOLDRICK, P., RAINBIRD, R. H., . . . LYONS, T. W. (2014). Low mid-Proterozoic atmospheric oxygen levels and the delayed rise fo animals *Science, 346*(6209), 4. doi: 10.7910/DVN/27366

REINHARD, C. T., PLANAVSKY, N. J., WANG, X., FISCHER, W. W., JOHNSON, T. M., & LYONS, T. W. (2014). The isotopic composition of authigenic chromium in anoxic marine sediments: A case study from the Cariaco Basin. *Earth and Planetary Science Letters, 407*, 9-18. doi: 10.1016/j.epsl.2014.09.024

RODLER, A., SÁNCHEZ-PASTOR, N., FERNÁNDEZ-DÍAZ, L., & FREI, R. (2015). Fractionation behavior of chromium isotopes during coprecipitation with calcium carbonate: Implications for their use as paleoclimatic proxy. *Geochimica et Cosmochimica Acta, 164*, 221-235. doi: 10.1016/j.gca.2015.05.021

SAAD, E. M., WANG, X., PLANAVSKY, N. J., REINHARD, C. T., & TANG, Y. (2017). Redox-independent chromium isotope fractionation induced by ligand-promoted dissolution. *Nat Commun, 8*(1), 1590. doi: 10.1038/s41467-017-01694-y

SAMANTA, M., ELLWOOD, M. J., & MORTIMER, G. E. (2016). A method for determining the isotopic composition of dissolved zinc in seawater by MC-ICP-MS with a 67 Zn– 68 Zn double spike. *Microchemical Journal, 126*, 530-537. doi: 10.1016/j.microc.2016.01.014

SCHMID, S. (2015). Sedimentological review of the Barney Creek Formation in drillholes LV09001, BJ2, McA5, McArthur Basin. In G. MacDonald. (Ed.), *Record*. Darwin: Northern Territory Geological Survey.

SCHOENBERG, R., ZINK, S., STAUBWASSER, M., & VON BLANCKENBURG, F. (2008). The stable Cr isotope inventory of solid Earth reservoirs determined by double spike MC-ICP-MS. *Chemical Geology, 249*(3-4), 294-306. doi: 10.1016/j.chemgeo.2008.01.009

SHEEN, A. I., KENDALL, B., REINHARD, C. T., CREASER, R. A., LYONS, T. W., BEKKER, A., . . . ANBAR, A. D. (2018). A model for the oceanic mass balance of rhenium and implications for the extent of Proterozoic ocean anoxia. *Geochimica et Cosmochimica Acta, 227*, 75-95. doi: 10.1016/j.gca.2018.01.036

TANG, D., SHI, X., WANG, X., & JIANG, G. (2016). Extremely low oxygen concentration in mid-Proterozoic shallow seawaters. *Precambrian Research, 276*, 145-157. doi: 10.1016/j.precamres.2016.02.005

YANG, B., SMITH, M., COLLINS, A. S., MUNSON, T. J., SCHOEMAKER, B., NICHOLLS, D., . . . GLORIE, S. (2018). Spatial and temporal variation in detrital zircon age provenance of the hydrocarbon-bearing upper Roper Group, Beetaloo Sub-basin, Northern Territory, Australia. *Precambrian Research, 304*, 140-155. doi: 10.1016/j.precamres.2017.10.025

YANG, S., KENDALL, B., LU, X., ZHANG, F., & ZHENG, W. (2017). Uranium isotope compositions of mid-Proterozoic black shales: Evidence for an episode of

increased ocean oxygenation at 1.36 Ga and evaluation of the effect of post-depositional hydrothermal fluid flow. *Precambrian Research, 298*, 187-201. doi: 10.1016/j.precamres.2017.06.016

ZHANG, S., WANG, X., WANG, H., BJERRUM, C. J., HAMMARLUND, E. U., COSTA, M. M., . . . CANFIELD, D. E. (2016). Sufficient oxygen for animal respiration 1,400 million years ago. *Proc Natl Acad Sci U S A, 113*(7), 1731-1736. doi: 10.1073/pnas.1523449113

ZHU, S., ZHU, M., KNOLL, A. H., YIN, Z., ZHAO, F., SUN, S., . . . LIU, H. (2016). Decimetre-scale multicellular eukaryotes from the 1.56-billion-year-old Gaoyuzhuang Formation in North China. *Nat Commun, 7*, 11500. doi: 10.1038/ncomms11500

SUPPLEMENTARY INFORMATION

Cr-Purification Chromatography

TUNGSTEN CARBIDE RING MILL

The samples were powdered using a Rocklabs tungsten carbide ring mill until the powder no longer feels gritty for consistency in sizes. A standard procedural cleaning step of crushing quartz grains and cleaning the tungsten carbide crucible with ethanol were performed between crushing samples to ensure prevention of cross contamination.

ACIDS AND LABORATORY MATERIALS

All chemistry was performed inside Class 100 chemical workstations located inside a suited of Class 1000 over-pressured ultraclean laboratory in the basement of the Mawson Building, University of Adelaide. All AR grade acids (e.g. HCl, HNO_3 and HF) were purified by David Bruce, the laboratory manager using Savillex™ DST-1000 sub-boiling distillation system. Ultrapure Milli-Q H_2O with an 18.2MΩ cm^{-1} resistivity was accessed using a Millipore Element system and was used throughout this project. The Nb_2O_5 compound with the exact purity of 99.99% was obtained from the Puratronic Company, 110mg in a solution of 5mL of 0.40M H_3PO_4. All Savillex™ PFA Teflon vials were pre-cleaned with heated recycled ~6M HCl, ~6M AR Grade HNO_3, ~6M AR Grade HCl, Milli-Q H_2O and Single-Distilled 6M HCl for 1day before being used for any chemical treatment and storage.

COMPLETE DIGESTING, LEACHING AND, MAJOR AND TRACE ELEMENT ANALYSIS

Before performing Cr-purification chromatography on the samples, their Cr/Al and Cr/Ti ratios were first analysed and compared to that of the 'Average Shale'. Ratio values higher than that of the 'Average Shale' would indicate that the $\delta^{53}Cr$ on these samples are more likely dominated by authigenic Cr rather than detrital factors. The samples were leached with 3M HNO_3 for 24hrs (Reinhard et al., 2014) in a rotating table before being sent to the QQQ-ICP-MS in Adelaide Microscopy for Major and Trace Element Analysis. Once the data were obtained, 'data reduction' was performed to obtain the Cr/Al and Cr/Ti ratios which were then compared to that of the shale standards.

$^{50\text{-}54}$CR DOUBLE SPIKE

Of the samples with high Cr/Al and/or Cr/Ti relative to the 'Average Shale', fresh new powders were obtained, double spiked and leached for Cr-purification Chromatography. The amount of double spike added to the samples were determined from the Cr concentrations from the major and trace elements data. The $^{50\text{-}54}$Cr double spike was added with the first acid used for leaching to take into account the possible loss of Cr and potential $\delta^{53}Cr$ fractionation that may occur during the leaching and Cr-purification

Chromatography to produce a $\delta^{53}Cr$ signature that is representative of authigenic Cr from the rock and not values resulted from chromatography.

CHROMIUM-PURIFICATION CHROMATOGRAPHY

Isolating Cr from the matrix elements required a two-step double spiked Cr-purification chromatography adapted from (Paulukat, 2016). Bio-Rad AG® 1-X8 anion-exchange resin ($100-200$mesh, Bio-Rad Laboratories) and Bio-Rad AG® 50W-X8 cation exchange resin ($200-400$mesh, Bio-Rad Laboratories) were used to isolate Cr from the rock matrix. The cleaning step for each resin before use are as follows:

Cleaning Anion Resin

- Avoid using metal spatula when scooping fresh resin
- Store Resin in ~6M HCl, ensure resin is completely submerged.
- Replace ~6M HCl with new one every 2days, repeat 5times.
- Transfer resin in large 20mL Bio-Rad chromatography resin
- Sequentially pass MQ 5×, ~5M HNO3 5×, MQ 5×, ~6M HCl 5× and MQ 5×
- Store in ~6M HCl in a new clean container

Cleaning Cation Resin

- Avoid using metal spatula when scooping fresh resin
- Transfer resin in large 20mL Bio-Rad chromatography resin
- Sequentially pass MQ 5×, ~5M HNO_3 5×, MQ 5×, ~6M HCl 5× and MQ 5×
- Store in ~0.5M HCl in a new clean container

ANION COLUMN

After leaching, the samples were heated to boil to oxidise for an hour with 0.5mL of 0.2M $(NH_4)_2S_2O_8$ (ammonium persulfate) and 1M HCl before being passed through the anion exchange resin. About $\sim 2/3$ of the Poly-Prep® Bio-Rad column stems were filled with the Bio-Rad AG® 1-X8 anion-exchange resin which were sequentially pre-cleaned with ~5M HNO_3, Milli-Q H_2O and ~6M HCl, Milli-Q H_2O and conditioned with 0.1M HCl before sample loading. Oxidised Cr(VI) adheres strongly to the resin while most of the matrix was eluted with 10mL of 0.2M HCl, 2mL of 2M HCl and Milli-Q H_2O. Elution of Cr was done by 10mL of 2M HNO_3 and ~0.3mL of 5% H_2O_2 with another 5mL of 2M HNO_3 and ~.7mL of 5% H_2O_2, strongly adapted from (Paulukat, 2016).

CATION COLUMN

The samples were dried and $\sim 1/3$ of the polypropylene Evergreen Scientific column stem were filled with Bio-Rad AG® 50W-X8 cation exchange resin which were pre-cleaned with Milli-Q H_2O, ~5M HNO_3, Milli-Q H_2O ~6M HCl, Milli-Q H_2O and conditioned with 0.5M HCl, adapted from (Paulukat, 2016). The dried samples were

dissolved into solution with 12M HCl and Milli-Q H_2O heated for ~10mins before being loaded and the final elution of Cr with 8mL of 0.5M HCl.

IRON COLUMN

Samples with high Fe concentrations were passed through an 'Iron Column' which isolates only iron before being passed through the anion exchange resin. The iron column is very similar to the first column where the same resin and the same columns were used in this procedure. The Fe Column step was sequentially pre-cleaned with ~5M HNO_3, Milli-Q H_2O and twice with ~6M HCl. The sample was slowly added 1mL at a time until completely poured and the all matrix, excluding Fe, was flushed with 1mL of double distilled HCl, 4times. The sample was later evaporated ready for the Anion column.
The Standard Operating Procedure for Cr-Purification Chromatography in the University of Adelaide was a product of this project (see end of 'Supplementary Information' section)

TIMS

The ^{50}V interference on ^{54}Cr was corrected using the IUPAC values of 1.04320 and 0.002503 for $^{49}Ti/^{50}Ti$ and $^{50}V/^{51}V$, respectively. The ^{54}Fe interference on ^{54}Cr was corrected using the IUPAC values of 0.063703 for the $^{54}Fe/^{56}Fe$.

QQQ-ICP-MS

A mixed Ca-Cr-Fe-K-Mn-V-Ti standard solution was used in this procedure which contains 2µg of each element. It was passed through column chemistry, treated identically as other rock samples. An Agilent Technologies 8900 ICP-MS Triple Quad was used to analyse the concentration of the ^{52}Cr.

δ^{53}CR ANALYSES

Table 3. Summarised δ^{53}Cr (‰) results with corresponding Formation, Lithology, Stratigraphic Depth (m) and Age (Gyr) of all the samples in this project.

Formation	Depth	δ53Cr	2SE	Cr (ppm)	Frei's δ53(	Frei's 2SE	Frei's Cr (p
Undiffere	485.75	1.389184	0.038415	9.768685	1.37	0.027	7.324
Reward D	558.75	-	-	-	0.237	0.064	0.475
Reward D	619.1	0.034897	0.032904	0.386742	0.251	0.034	0.424
Reward D	642.7	-	-	-	0.227	0.032	0.546
Reward D	666.7	0.246149	0.096087	0.452349	0.246	0.096	0.693
Reward D	704.4	-	-	-	-0.152	0.045	0.958
Reward D	705.9	-0.02536	0.044158	1.361969	-0.035	0.045	1.385
Reward D	707.2	-	-	-	-0.153	0.058	1.989
Fraynes F	708.4	-	-	-	-0.068	0.046	2.964
Fraynes F	729.9	-	-	-	-0.018	0.032	1.719
Fraynes F	755.6	-0.03025	0.040968	1.872152	-0.185	0.037	1.616
Campbell	801.1	-	-	-	0.13	0.052	1.872
Campbell	883.7	-0.24273	0.045183	3.015147	-0.072	0.036	1.096
Campbell	899.3	-	-	-	0.058	0.056	0.795
Campbell	932.5	-0.03167	0.042849	1.073027	0.04	0.048	1.015
Campbell	950.6	-	-	-	-0.293	0.028	2.173
Campbell	977.7	0.007057	0.040808	0.882999	-0.112	0.063	0.858
Blue Hole	1008.9	-	-	-	-0.091	0.052	1.344
Blue Hole	1040.6	-0.10217	0.041017	1.016718	0.157	0.054	1.274
Blue Hole	1052.5	-	-	-	-0.163	0.045	0.799

Formatior	Depth	d53Cr	2SE	Cr (ppm)	Frei's d53(	Frei's 2SE	Frei's Cr (p	Cycles
Donnegan	210	-0.10854	0.044115	5.559829	0.077	0.038	1.397	130
Donnegan	252.55	-0.20148	0.040027	1.601731	-0.115	0.065	1.723	200
Hot Spring	279.35	-	-	-	-0.080	0.030	3.013	-
Hot Spring	289.85	-	-	-	-0.065	0.039	2.862	-
Hot Spring	294.3	-0.1732	0.048593	1.944292	-0.185	0.039	1.984	150
Hot Spring	301.05	-	-	-	0.022	0.047	4.504	-
Reward D	313.43	0.003754	0.042477	1.605735	-0.148	0.029	1.612	200
Reward D	318.6	-	-	-	-0.085	0.054	1.842	-
Reward D	330.4	-	-	-	-0.067	0.048	3.655	-
Reward D	341.1	-0.07843	0.044306	2.233768	-0.087	0.040	2.769	150
Reward D	360.2	-	-	-	-0.111	0.054	1.623	-
Barney Cr	375.85	0.076394	0.041648	1.825524	0.076394	0.041648	1.825524	200
Barney Cr	393.7	-0.07527	0.043974	3.453042	-0.07527	0.043974	3.453042	200
Barney Cr	412.88	-0.19538	0.044253	3.90078	-0.19538	0.044253	3.90078	200
Barney Cr	419.66	-0.25146	0.045489	2.713454	-0.25146	0.045489	2.713454	175
Barney Cr	445	-0.13655	0.056551	4.394711	-0.13655	0.056551	4.394711	175
Barney Cr	463.6	-0.06965	0.061271	4.527492	-0.06965	0.061271	4.527492	150
Barney Cr	490.7	-0.13936	0.054696	4.290774	-0.13936	0.054696	4.290774	150
Barney Cr	502.5	0.409119	0.062654	2.409593	0.409119	0.062654	2.409593	160
Barney Cr	515	-0.08608	0.046064	4.356891	-0.08608	0.046064	4.356891	200
Cooley Br	530	-	-	-	-0.017	0.053	3.958	-
Cooley Br	534.25	-0.07047	0.050791	5.611966	-0.163	0.040	5.571	200
Cooley Br	540.02	-	-	-	-0.137	0.039	5.479	-
Cooley Br	543	-	-	-	-0.034	0.048	5.216	-
Teena Dol	554.1	-	-	-	-0.049	0.056	4.429	-
Teena Dol	567.5	-	-	-	-0.145	0.045	5.772	-
Emmerug	592.48	-0.18295	0.062976	9.441151	-0.048	0.040	9.685	150
Emmerug	601.7	-0.03441	0.05387	4.672151	-0.080	0.049	4.488	150
Emmerug	603.83	-0.02256	0.044023	2.638076	-0.084	0.056	2.691	200

Cr-Purification Chromatography Standard Operating Procedure

Day 1 (Sample Preparation)

Evaporate sample solution in a 30mL tall Teflon beaker at 130°C	
Add ~2mL of fresh *Aqua Regia (3:1 ratio=~12M HCl to ~11M HNO_3)* on dried sample and evaporate again at 130°C	
Add 20mL of MQ to each of the sample to dissolve it overnight, at room temperature	

Day 2 (Bio-Rad AG® 1-X8; 100 – 200 mesh. *Poly-Prep® Bio-Rad columns)*

Before Cleaning the column:	
Weigh ~230mg of Ammonium Persulfate (APDS) to dissolve in 5mL of MQ. Shake thoroughly. Avoid using a metal spatula.	
To each sample vial: add 0.5mL of APDS solution and 0.5mL of 1M HCl. Dispose remaining APDS after use.	
Dissolve samples at 170°C, for 1hr. Start timing when the first sample boils and lower temperature to 130°C slightly after 30mins of boiling.	
Rapidly cool vials by partially submerging in cold tap H_2O for ~5mins.	
Cleaning Procedure (while boiling samples):	
Add ~$^2/_3$ of *settled* Anion resin on column stem	
Add ~1 reservoir of MQ	
Add ~1 reservoir of ~5M HNO_3	
Add ~1 reservoir of MQ	
Add ~1 reservoir of ~6M HCl	
Add ~1 reservoir of MQ	
Add 1 reservoir of 0.1M HCl	
Load cooled samples*	
Flush matrix with 10mL of 0.2M HCl	
Add 2mL of 2M HCl	
Add ~$^1/_2$ reservoir of MQ	
Place clean vials underneath columns	
Collect Cr with 1mL of 2M HNO_3 and 3 drops of 5% H_2O_2	
Wait ~5mins	
Add 5mL of 2M HNO_3 and 7 drops of 5% H_2O_2	
Evaporate samples overnight at 130°	
Transfer anion resin to a 'used anion resin' container and store in ~6M HCl	
Store Poly-Prep frits in H_2O; columns can be re-used as much as needed	

Day 3 (Fe Column; only for Fe-rich samples), if not continue to **Day 4**. Same column and Resin as **Day 2**.

Cleaning Procedure	
Add ~$^2/_3$ of *settled* Anion resin on column stem	
Add ~1 reservoir of Milli-Q H_2O	
Add ~5mL of ~5M HNO_3	
Add ~5mL of MQ	
Add ~5mL of ~0.2M HCl	
Add ~5mL of ~6M HCl	
Add ~5mL of ~6M HCl (again)	
Add 1mL of 6M HCl to evaporated sample and supersonic for ~2min	
Place new clean Teflon beaker underneath columns, then load sample	
Add 1mL of 6M HCl (double distilled preferably, but not essential)	
Add 1mL of 6M HCl (double distilled preferably, but not essential)	
Add 1mL of 6M HCl (double distilled preferably, but not essential)	
Add 1mL of 6M HCl (double distilled preferably, but not essential)	
Evaporate samples overnight at 130°C	

Transfer anion resin to a 'used anion resin' container and store in ~6M HCl	
Store Poly-Prep frits in H_2O; columns can be re-used as much as needed	

Day 4 (Bio-Rad AG® 50W-X8; 200 – 400 mesh. *Evergreen Scientific columns*)

Cleaning Procedure:	
Add ~ $^1/_3$ of *settled* Cation resin on column stem	
Add ~1 reservoir of MQ	
Add ~1 reservoir of ~5M HNO_3	
Add ~1 reservoir of MQ	
Add ~1 reservoir of ~6M HCl	
Add ~1 reservoir of MQ	
Add ~ $^1/_2$ reservoir of 0.5M HCl	
Make Activator:	
Add 100µL of 12M HCl to each sample and heat on the hotplate at 130°C, uncapped for ~10mins	
Add 2.3mL of MQ to each sample	
Place new clean Teflon beaker underneath columns, then load sample	
Add 8mL of 0.5M HCl* and evaporate at 130°C overnight	
Transfer cation resin to a 'used cation resin' container and store in ~0.5M HCl	
Store Evergreen frits in H_2O; columns can be re-used as much as needed	

Notes: (Read before performing Chromatography)

- Evergreen columns must be double-fritted, add an additional 1 Eichrom® frit to each column using a Teflon rod before using for the first time.
- First time using Evergreen column, store frits in ~0.1M HNO_3 for at least 48hrs. The longer the better.
- ***** while acids and sample solutions should be fully drained before resuming to the next step, these steps permit adding more acids and sample solutions even when partially drained.
- ~ means concentration or volume does not necessarily need to be accurate, anything else must be accurate.

Day 1 homogenises the samples
Day 2 elutes ideally only Cr and flushes the rest of the matrix elements (i.e. Mn, V, Ti, Fe, etc.)
Day 3 removes the excess Fe in the samples
Day 4 adheres the remaining trace matrix elements on the resin and elutes only Cr
Refer to the Table 3 in the Supplementary Information of Canfield et al. (2018).

Sample	Depth (m	Mg (ppb)	Al(ppb)	P(ppb)	Ca(ppb)	Cr(ppb)	Mn (ppb)	Fe(ppb)	Cu (ppb)	Zn(ppb)	Sr(ppb)	Ba (ppb)	87Sr/86Sr
LV55	210	232344.9	31463.2	926.7	401490.5	89.1	8276.12	29092.6	7.989	58.432	531.856	302.106	0.7246
LV51	253	193753.5	21717.5	903.5	376890.2	41.1	5070.22	23344.4	12.027	17.515	255.492	289.631	0.7288
LV43	294.3	527930.3	6619.2	649.6	1126905	26.46	14362.74	30018.4	19.418	64.401	252.405	191.444	0.7152
LV41	313.43	356133.1	12600.8	711	781564.7	13.79	11713.04	38445.3	4.313	17.519	496.356	206.897	0.7154
LV38	341.1	540907.8	3190.8	546.2	1176808	62.02	18552.15	41920.5	12.873	28.329	982.716	111.337	0.707
LV34	375.85	349916	7316.2	636.5	740249.2	54.84	8541.57	33618.3	3.814	35.838	489.688	244.112	0.7082
LV30	393.7	217083.2	9553.4	744.4	426760.8	11.49	8864.02	34345.7	26.76	10.609	368.791	205.737	0.7152
LV27	412.88	349960.6	9899.1	1668.2	763417.1	29.53	10185.85	36672.7	12.564	18.193	229.623	321.092	0.7257
LV26	419.66	339012	14008.7	4050.7	756163.5	31.94	8868.45	46740.4	26.866	23.952	219.599	408.22	0.736
LV24	445	426699.3	11963.3	1048.5	935447.9	40.84	12308.98	63920.9	25.031	49.316	295.557	319.303	0.7221
LV20	463.6	298587.2	11816.1	1820.9	664778.9	29.85	16505.46	39495.7	23.999	44.63	366.798	363.828	0.7227
LV18	490.7	265561.9	11714.4	3226	580584.1	40.61	12670.62	36271.8	15.266	46.589	304.376	348.604	0.7237
LV17	502.5	79344.9	13174.1	2041.4	161347.2	18.12	2413.61	27363.1	11.715	61.78	207.428	394.958	0.7337
LV15	515	353492.4	8852.8	1050.3	772521.4	34.69	6486.7	45281.9	10.915	134.133	649.514	235.617	0.7109
LV13	534.25	535431.2	9198.5	889.2	1110369	69.33	10061.74	41802.6	8.076	15.709	196.99	173.301	0.7169
LV3	592.48	578918.2	5440.3	1294.4	1208953	116.26	10187.41	45379.6	15.417	59.131	298.276	143.373	0.7094
LV2	601.7	653795.3	4019.7	1345.5	1339828	75.17	5842.62	32742.4	15.706	29.047	433.485	111.892	0.7071
LV1	603.83	605457.2	1812.5	602.2	1214758	25.19	4537.26	21529.6	8.417	34.471	376.026	51.926	0.7062

Figure 22. Elemental analyses of leachate samples from McArthur Samples.

Depth (m)	Al(ppm)	p(ppm)	K(ppm)	Mn(ppm)	Fe (ppm)	Cu (ppm)	Rb(ppm)	Sr (ppm)	Mg(ppm)	Ca (ppm)	87/86 Sr	2se for 87/86 Sr
485.75	59.22752	8.902768	22.0764	2135.346	2988.451	0.844129	BDL	22.74314	127224.9	173028.4	0.707043	0.000012
558.75	57.58981	4.125094	15.21544	2178.407	3397.769	2.311487	BDL	16.1948	101234.2	132527.3	0.707111	0.000005
619.1	98.87622	7.87676	24.16464	2418.743	2090.669	1.67279	BDL	15.2008	102233.9	132561.6	0.708052	0.000012
642.7	109.3641	6.868489	16.74245	1789.037	3710.094	0.908601	BDL	11.25494	104284.8	127719.1	0.707402	0.000006
666.7	128.7498	5.25385	9.202534	1573.879	2153.672	0.869992	BDL	9.800583	90291.13	122457.8	0.707545	0.000018
704.4	506.2067	10.72527	109.2237	2512.244	9194.304	1.489229	BDL	18.85588	197604.3	257070.6	0.709495	0.000014
705.9	245.2256	7.408066	39.23258	1621.029	6301.449	0.449333	BDL	11.16343	109674.4	146268.4	0.707841	0.000007
707.2	234.4378	9.583486	45.8839	995.6957	4697.358	0.300738	BDL	6.53286	74728.12	101468.1	0.709342	0.000006
708.4	900.3545	10.26328	299.606	857.8497	4192.005	0.519979	0.388654	7.710029	58451.91	79949.5	0.721634	0.000007
729.9	781.6738	17.90583	180.2757	666.6174	7582.156	0.696355	0.411079	52.05106	63566.05	204452.5	0.71113	0.000004
755.6	326.185	8.499731	90.40946	539.0451	2852.955	0.090392	0.129746	20.19736	15542.96	68249.55	0.710993	0.000004
801.1	253.152	11.32539	72.93757	287.3127	4779.469	BDL	BDL	4.429295	37248.25	59583.28	0.720968	0.000011
883.7	343.6244	45.00021	5.098613	657.4062	6526.649	0.534339	BDL	60.19429	116201.3	161659.8	0.705383	0.000004
899.3	338.6968	15.94206	BDL	1086.112	4011.715	0.134758	BDL	65.30797	124773.1	179706.9	0.705161	0.000003
932.5	577.5197	14.39188	BDL	1320.255	3525.676	0.333713	BDL	36.86268	111707.3	142496.9	0.705803	0.000006
950.6	415.8493	12.33591	BDL	2440.335	4814.622	0.775758	BDL	33.15134	122219.4	158343.1	0.706197	0.000004
977.7	345.4435	16.5485	BDL	1205.949	5355	0.392686	BDL	33.54708	105506	150333.9	0.706434	0.000007
1003.9	701.7281	43.79216	102.0661	1300.069	7302.017	0.818516	0.271225	50.43708	109160.3	150388.6	0.708386	0.000005
1040.6	542.8998	7.938009	104.2638	1467.882	13762.43	0.187887	0.347502	18.2907	92233.63	124781.7	0.713059	0.000006
1052.5	947.1958	10.1298	143.8765	3549.993	4326.291	1.397722	0.388619	26.0626	117296.5	149740.5	0.714958	0.000009

Depth (m)	La(ppm)	Ce (ppm)	Pr(ppm)	Nd(ppm)	Sm (ppm)	Eu(ppm)	Gd(ppm)	Tb (ppm)	Dy (ppm)	Ho(ppm)	Er(ppm)	Tm (ppm)	Yb (ppm)
485.75	1.486254	3.372975	0.418949	1.534885	0.346888	0.072059	0.456051	0.051847	0.219274	0.039433	0.083373	0.012504	0.064328
558.75	0.318118	1.064493	0.167412	0.752181	0.439363	0.126516	0.879228	0.109446	0.426343	0.065566	0.137762	0.021042	0.106707
619.1	0.349108	0.997725	0.135356	0.633701	0.317389	0.095376	0.612159	0.066308	0.264992	0.03386	0.073389	0.008637	0.042858
642.7	0.350679	0.911228	0.128265	0.517031	0.200027	0.051999	0.39922	0.036125	0.162094	0.025029	0.047842	0.005729	0.030563
666.7	0.381376	0.927284	0.126569	0.435685	0.124046	0.031267	0.204873	0.022471	0.102244	0.017218	0.048373	0.005349	0.032149
704.4	2.114393	4.708905	0.55587	2.072566	0.369818	0.08671	0.458404	0.053668	0.281701	0.053073	0.13994	0.019064	0.116767
705.9	1.602373	3.584988	0.408896	1.545945	0.286958	0.050211	0.258134	0.036708	0.211301	0.036182	0.107644	0.014977	0.089064
707.2	0.954231	2.189162	0.280982	1.017137	0.204234	0.035917	0.205406	0.025179	0.151834	0.026138	0.070015	0.012182	0.059594
708.4	1.689	4.313724	0.554474	1.992407	0.411265	0.075896	0.377165	0.057571	0.343987	0.069651	0.19854	0.0294	0.21125
729.9	20.65125	43.85978	4.897603	16.43221	2.530758	0.367533	1.992276	0.265815	1.364695	0.257969	0.712451	0.091661	0.577234
755.6	5.255767	11.96561	1.261853	4.363922	0.731616	0.121206	0.582226	0.080956	0.451042	0.083601	0.229009	0.032282	0.205872
801.1	2.545604	6.804082	1.110443	4.698645	0.910658	0.176816	0.723181	0.090693	0.447383	0.082784	0.213662	0.025279	0.164629
883.7	1.514818	3.249995	0.396816	1.521848	0.32074	0.076316	0.355998	0.046389	0.212731	0.038168	0.112935	0.01203	0.089381
899.3	1.347967	3.633315	0.477726	1.888473	0.518702	0.136231	0.660242	0.081435	0.371599	0.062322	0.14242	0.016636	0.086794
932.5	1.657662	4.454118	0.588659	2.21195	0.616023	0.139609	0.772499	0.096416	0.517522	0.091078	0.234205	0.031716	0.20134
950.6	0.955764	3.083289	0.45228	2.077312	0.70726	0.173104	0.888444	0.132965	0.745853	0.133395	0.339711	0.04285	0.293879
977.7	2.271837	6.631733	0.912487	3.61706	0.923147	0.202422	1.0799	0.139668	0.648007	0.108921	0.286633	0.030521	0.175603
1003.9	2.210853	8.915629	1.500504	7.418771	2.598731	0.610928	2.988517	0.486666	2.666968	0.451824	1.101138	0.125439	0.71593
1040.6	6.812387	18.1257	2.442803	9.2832	1.778655	0.294199	1.671792	0.230155	1.273648	0.245889	0.619582	0.068424	0.424758
1052.5	3.823145	14.76295	2.430894	10.45565	2.41433	0.457311	2.480946	0.337315	1.77407	0.335594	0.87554	0.109747	0.637809

Figure 23. Elemental analyses of leachate samples from Limbunya Samples.

SUPPLEMENTARY INFORMATION REFERENCES

CANFIELD, D. E., ZHANG, S., FRANK, A. B., WANG, X., WANG, H., SU, J., . . . FREI, R. (2018). Highly fractionated chromium isotopes in Mesoproterozoic-aged shales and atmospheric oxygen. *Nat Commun*, *9*(1), 2871. doi: 10.1038/s41467-018-05263-9

PAULUKAT, C. (2016). Chromium stable isotope fractionation in modern biogeochemical cycling: Insights from continental weathering flux to the ocean, and chromium incorporation into carbonate shells. (Ph.D), University of Copehagen.

REINHARD, C. T., PLANAVSKY, N. J., WANG, X., FISCHER, W. W., JOHNSON, T. M., & LYONS, T. W. (2014). The isotopic composition of authigenic chromium in anoxic marine sediments: A case study from the Cariaco Basin. *Earth and Planetary Science Letters, 407*, 9-18. doi: 10.1016/j.epsl.2014.09.024